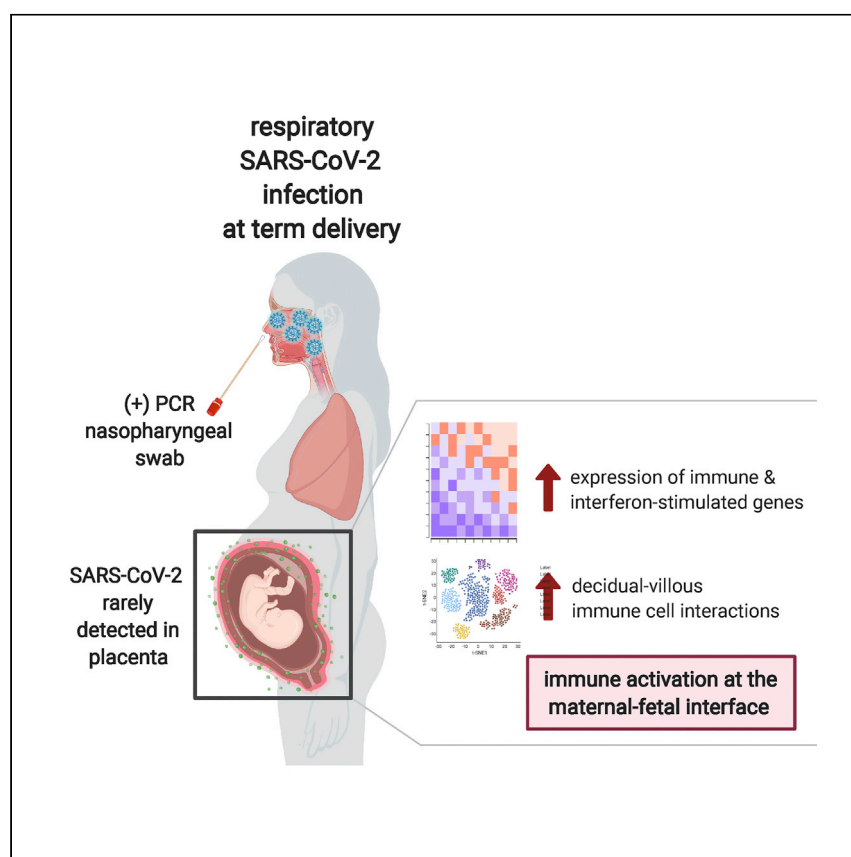# Med

Clinical and Translational Article

Maternal respiratory SARS-CoV-2 infection in pregnancy is associated with a robust inflammatory response at the maternal-fetal interface

Alice Lu-Culligan, Arun R. Chavan, Pavithra Vijayakumar, ..., Harvey J. Kliman, Akiko Iwasaki, Shelli F. Farhadian

akiko.iwasaki@yale.edu (A.I.)
shelli.farhadian@yale.edu (S.F.F.)

Highlights

Most women with SARS-CoV-2 at delivery had no detectable viral RNA at the placenta

ACE2 is highly expressed in the placenta during early pregnancy but rarely at term

Placental cytotrophoblasts are susceptible to SARS-CoV-2 infection *in vitro*

RNA-seq reveals robust placental immune activation during maternal SARS-CoV-2 infection

COVID-19 is more severe in pregnant women and can lead to adverse fetal outcomes. Through histological and gene expression studies of placentas from infected women, Lu-Culligan et al. find that maternal SARS-CoV-2 infection during term pregnancy and delivery is associated with immune activation at the maternal-fetal interface even in the absence of detectable virus in the placenta.

Translation to Patients

Med

Clinical and Translational Article

Maternal respiratory SARS-CoV-2 infection in pregnancy is associated with a robust inflammatory response at the maternal-fetal interface

Alice Lu-Culligan,[1] Arun R. Chavan,[1] Pavithra Vijayakumar,[2] Lina Irshaid,[3] Edward M. Courchaine,[4,5] Kristin M. Milano,[2] Zhonghua Tang,[2] Scott D. Pope,[1] Eric Song,[1] Chantal B.F. Vogels,[6] William J. Lu-Culligan,[4,5] Katherine H. Campbell,[2] Arnau Casanovas-Massana,[6] Santos Bermejo,[7] Jessica M. Toothaker,[8,9] Hannah J. Lee,[1] Feimei Liu,[1] Wade Schulz,[10] John Fournier,[11] M. Catherine Muenker,[6] Adam J. Moore,[6] Yale IMPACT Team, Liza Konnikova,[2,8] Karla M. Neugebauer,[4] Aaron Ring,[1] Nathan D. Grubaugh,[6] Albert I. Ko,[6] Raffaella Morotti,[3] Seth Guller,[2] Harvey J. Kliman,[2] Akiko Iwasaki,[1,12,13,*] and Shelli F. Farhadian[11,14,*]

SUMMARY

Background: Pregnant women are at increased risk for severe outcomes from coronavirus disease 2019 (COVID-19), but the pathophysiology underlying this increased morbidity and its potential effect on the developing fetus is not well understood.

Methods: We assessed placental histology, ACE2 expression, and viral and immune dynamics at the term placenta in pregnant women with and without respiratory severe acute respiratory syndrome coronavirus 2 (SARS-CoV-2) infection.

Findings: The majority (13 of 15) of placentas analyzed had no detectable viral RNA. ACE2 was detected by immunohistochemistry in syncytiotrophoblast cells of the normal placenta during early pregnancy but was rarely seen in healthy placentas at full term, suggesting that low ACE2 expression may protect the term placenta from viral infection. Using immortalized cell lines and primary isolated placental cells, we found that cytotrophoblasts, the trophoblast stem cells and precursors to syncytiotrophoblasts, rather than syncytiotrophoblasts or Hofbauer cells, are most vulnerable to SARS-CoV-2 infection *in vitro*. To better understand potential immune mechanisms shielding placental cells from infection *in vivo*, we performed bulk and single-cell transcriptomics analyses and found that the maternal-fetal interface of SARS-CoV-2-infected women exhibited robust immune responses, including increased activation of natural killer (NK) and T cells, increased expression of interferon-related genes, as well as markers associated with pregnancy complications such as preeclampsia.

Conclusions: SARS-CoV-2 infection in late pregnancy is associated with immune activation at the maternal-fetal interface even in the absence of detectable local viral invasion.

Context and significance

Pregnant women with COVID-19 are at increased risk for severe illness and pregnancy complications compared with non-pregnant women. Researchers at Yale School of Medicine analyzed placentas from SARS-CoV-2-infected women at the time of delivery and found that, although placental cells are susceptible to infection *in vitro*, viral RNA is rarely detected in clinical samples. The Yale team observed local immune responses at the maternal-fetal interface, including upregulation of interferon pathways and activation of T and NK cells. Although placental immune activation during maternal SARS-CoV-2 infection likely represents a host defense mechanism of shielding the maternal-fetal interface from infection, these inflammatory changes may contribute to the increased risk for complications seen in COVID-19-affected pregnancies.

INTRODUCTION

Coronavirus disease 2019 (COVID-19), resulting from severe acute respiratory syndrome coronavirus 2 (SARS-CoV-2) infection, is a public health emergency that has affected the lives of millions of people around the world. The effect of SARS-CoV-2 infection in pregnant women is of particular concern; population-based studies suggest that pregnant women with COVID-19 are at increased risk for severe illness compared with non-pregnant women with COVID-19.[1] SARS-CoV-2 infection during pregnancy has also been associated with increased risk of pregnancy complications, such as preterm birth, premature rupture of membranes, and preeclampsia.[2–4] However, the mechanisms underlying these poor outcomes are unknown, and their dependence on active SARS-CoV-2 infection of the placenta remains poorly understood. Given that pregnancy involves a tightly regulated series of immunological processes, perturbation of this environment may contribute to development of these pathologies. Although systemic inflammatory changes in maternal SARS-CoV-2 infection have been explored,[5] the inflammatory changes of the maternal-fetal interface during SARS-CoV-2 infection in pregnancy have yet to be elucidated. The emerging picture of the inflammatory consequences of SARS-CoV-2 infection during pregnancy suggests that exposed neonates could be at potential risk of long-term effects.[5,6]

Studies of other coronaviruses suggest a potential for placental pathology during maternal coronavirus infection through direct viral invasion at the placenta and through a secondary inflammatory reaction. Mouse hepatitis virus (MHV), a coronavirus of laboratory mice, infects placental cells in vivo,[7] leading to placental inflammation and increased susceptibility to subsequent bacterial infection of the placenta.[8] During the SARS pandemic of 2008, maternal infection with SARS-CoV-1 was associated with histological abnormalities but not with viral invasion of the placenta.[9] Case reports during the current COVID-19 pandemic have demonstrated that SARS-CoV-2 is capable of infecting the placenta;[10–12] however, the mechanism of viral entry remains unclear. Although variable findings have been reported,[13–17] recent transcriptomics analyses of healthy placentas have suggested limited expression of the canonical SARS-CoV-2 receptor ACE2 in the placenta and little to no co-expression of ACE2 with its classical co-factor TMPRSS2 at the transcriptional level.[13–15] Thus, it remains unclear whether the placenta is susceptible to SARS-CoV-2 infection under normal physiological conditions or under conditions of systemic inflammation, such as that occurring with maternal COVID-19. Moreover, it remains unknown whether placental pathology develops in the absence of viral infection of the placenta.[12,18,19]

In this study, we investigated the susceptibility of the human placenta to SARS-CoV-2 infection over the course of pregnancy through in situ analysis of ACE2 protein expression and in vitro studies. Furthermore, we describe in vivo immune responses at the maternal-fetal interface in response to maternal SARS-CoV-2 infection during full-term pregnancy.

RESULTS

SARS-CoV-2 infection of the placenta

Women who tested positive for SARS-CoV-2 infection by qRT-PCR of a nasopharyngeal swab or saliva at the time of delivery (n = 12, 80%) or in the 1 month prior to delivery (n = 3, 20%) were prospectively enrolled and consented to donation of biospecimens. One participant was identified based on positive SARS-CoV-2 testing at the time of delivery but was also noted to have an initial positive test 2 weeks prior. One pregnancy ended in fetal demise at 22 weeks;[12] the rest were full-term

[1]Department of Immunobiology, Yale School of Medicine, New Haven, CT, USA

[2]Department of Obstetrics, Gynecology, and Reproductive Sciences, Yale School of Medicine, New Haven, CT, USA

[3]Department of Pathology, Yale School of Medicine, New Haven, CT, USA

[4]Department of Molecular Biophysics and Biochemistry, Yale University, New Haven, CT, USA

[5]Department of Cell Biology, Yale School of Medicine, New Haven, CT, USA

[6]Department of Epidemiology of Microbial Diseases, Yale School of Public Health, New Haven, CT, USA

[7]Section of Pulmonary and Critical Care Medicine, Department of Medicine, Yale School of Medicine, New Haven, CT, USA

[8]Department of Pediatrics, Yale School of Medicine, New Haven, CT, USA

[9]Department of Immunology, University of Pittsburgh, Pittsburgh, PA, USA

[10]Department of Laboratory Medicine, Yale School of Medicine, New Haven, CT, USA

[11]Section of Infectious Diseases, Department of Medicine, Yale School of Medicine, New Haven, CT, USA

[12]Department of Molecular, Cellular and Developmental Biology, New Haven, CT, USA

[13]Howard Hughes Medical Institute, Chevy Chase, MD, USA

[14]Lead contact

*Correspondence: akiko.iwasaki@yale.edu (A.I.), shelli.farhadian@yale.edu (S.F.F.)

https://doi.org/10.1016/j.medj.2021.04.016

Table 1. Clinical features of COVID-19 cases tested by qRT-PCR

ID	Maternal age	Gestational age	Days between first positive test and delivery	Symptomatic COVID-19	Days between symptom onset and delivery	Treatment	Severe COVID-19[a]	NP swab SARS-CoV-2 RT-PCR at delivery	NP Swab CT value at delivery[b]	Placenta SARS-CoV-2 qRT-PCR
COVID 1	36	22.857	0	Y	0	HCQ	Y	+	33.8[c]	+
COVID 2	26	40.714	15	Y	19	no	Y	+	37.3[c]	−
COVID 3	32	38.143	1	Y	1	no	N	+	26.6	+
COVID 4	20	38.857	2	Y	2	no	Y	+	17.1	−
COVID 5	21	40.714	0	Y	21	no	N	+	43.8	−
COVID 6	35	41	1	N		no	N	+	30.4	−
COVID 7	22	40.286	2	N		no	N	+	39.3	−
COVID 8	31	39.429	1	N		no	N	+	31.9	−
COVID 9	34	41.143	0	N		no	N	+	35.5	−
COVID 10	40	37.714	4	N		no	N	+	37.5	−
COVID 11	36	38.286	27	Y	28	no	N	ND	ND	−
COVID 12	21	38.429	0	Y	7	no	N	+	32.7	−
COVID 13	35	39.714	1	N		no	N	+	22.2	−
COVID 14	36	36.857	24	Y	25	no	N	ND	ND	−
COVID 15	31	40.714	23	Y	40	no	N	ND	ND	−

ND, not done
[a]ICU or supplemental oxygen.
[b]N2 gene.
[c]Saliva.

deliveries. Overall, the median time from SARS-CoV-2 upper respiratory tract testing to placental sampling was 1.5 days (range, 0–28 days). One participant (COVID-1) received hydroxychloroquine; none of the other study participants received hydroxychloroquine, remdesivir, dexamethasone, or other treatment for COVID-19 prior to delivery. Clinical information about these participants is noted in Table 1.

Among the 15 placentas tested by qRT-PCR for the presence of SARS-CoV-2, viral RNA was detected in two of the placentas (Tables 1 and S1). One was from a 32-year-old woman who presented in labor at 38 weeks of gestation with symptoms of pneumonia, not requiring supplemental oxygen who progressed to a healthy delivery. The neonate tested negative for SARS-CoV-2 by nasopharyngeal swab qRT-PCR at the time of delivery. The other was from a woman who presented at 22 weeks of gestation with severe COVID-19 pneumonia and developed preeclampsia and fetal demise, resulting in fetal loss at 22 weeks. This case (COVID-1) was excluded from further histological and sequencing analyses presented here because the details of this case have been reported previously.[12] When we restricted our analysis to participants with full-term pregnancies who had a positive upper respiratory tract SARS-CoV-2 qRT-PCR at the time of full-term delivery, 1 of 11 had detectable viral RNA in the placenta. Plasma available for 12 SARS-CoV-2-infected women at the time of delivery was tested for systemic inflammatory markers and for SARS-CoV-2 spike S1 protein-specific immunoglobulin G (IgG) and IgM antibodies (anti-S1-IgG and -IgM). No apparent differences in ELISA absorbance values were observed between symptomatic and asymptomatic infected mothers or between pregnant and non-pregnant SARS-CoV-2-infected hospitalized individuals (Figures S1 and S2).

Histological features of COVID-19 cases
All women who delivered during the study period and who were diagnosed with SARS-CoV-2 infection by nasopharyngeal (NP) swab qRT-PCR at the time of or in the 1 month prior to delivery were retrospectively identified for inclusion in

Table 2. Clinical and demographic features of COVID-19 histological cases and controls

	All COVID-19 cases (n = 39)	Subset of COVID-19 cases with placenta histology available (n = 27)	Histological controls (n = 10)	ANOVA	p value
Age: median (range)	32 (18–41)	32.0 (18–41)	31.5 (21–37)	$F_{(1,47)} = 0.073$	0.788
Gestational age: median (range)	38 weeks 6 days (22 weeks 6 days–41 weeks 1 day)	39 weeks 0 days (36 weeks 6 days–41 weeks 1 day)	39 weeks 1 day (37 weeks–40 weeks 6 days)	$F_{(1,47)} = 0.208$	0.650
Comorbidities				Chi-square statistics	
Hypertension	31%	33%	40%	0.571	0.752
Preeclampsia	15%	19%	10%	0.892	0.640
Diabetes	26%	26%	20%	0.141	0.932
Mode of delivery (% CS)	33%	37%	30%	3.539	0.472
Sex of infant (% male)	50%	66%	40%	3.436	0.488
Gravidity: median (range)	3 (1–6)	2 (1–6)	3 (1–4)	ANOVA $F_{(1,47)} = 0.227$	0.636
Parity: median (range)	1 (0–4)	1 (0–4)	1 (0–3)	ANOVA $F_{(1,47)} = 0.006$	0.94
Neonatal Apgar, 1 min: median (range)	9 (4–9)	9 (4–9)	9 (4–9)	ANOVA $F_{(1,46)} = 2.561$	0.116
BMI: mean (SD)	33.0 (7.3)	33.4 (7.7)	27.1 (2.33)	ANOVA $F_{(1,47)} = 5.863$	**0.0194**
Race/ethnicity	African American: 23% Hispanic/Latino: 38% Non-Hispanic White: 31% Other: 8%	African American: 19% Hispanic/Latino: 33% Non-Hispanic White: 44% Other: 4%	African American: 10% Hispanic/Latino: 30% Non-Hispanic White: 40% Other: 20%	ANOVA $F_{(1,47)} = 0.031$	0.862
COVID-19 features				Chi-square Statistics	
COVID-19 symptoms at time of delivery (%)	56%	52%		0.261	
Maternal severe COVID-19[a]	13%	11%		0.996	
SARS-CoV-2 PCR testing of NP swab					
CT value:[b] median (range)	33.2 (17.1–43.8) (n = 26)	33.35 (17.1–43.8) (n = 18)			

[a]ICU or need for supplemental oxygen.
[b]N2 gene.

histological analyses (n = 39). Twenty-two (56%) of the SARS-CoV-2-infected women had symptomatic COVID-19. There were five cases of severe COVID-19 disease requiring administration of supplemental oxygen or intensive care unit (ICU) stay. Thirty-eight of the 39 pregnancies resulted in live births, with a median Apgar score of 9 (range, 4–9). Of the 39 total pregnant women with COVID-19 who delivered during the study period, 27 had placenta available for histological analyses (one COVID-19 case resulted in delivery of dizygotic twins; thus, 28 placentas were available for histological analysis). The COVID-19 placentas available for examination did not differ from the overall cohort of COVID-19 pregnancies during the study period by maternal age, maternal COVID-19 features, gestational age, mode of delivery, demographics, neonatal outcomes, or co-morbidities (Table 2).

Placental specimens were examined by two independent pathologists blinded to the individual's SARS-CoV-2 infection status and were assessed for the presence of villitis, chorioamnionitis, intervillositis, increased decidual lymphocytes, and fetal and maternal vascular malperfusion (Table S2; Data S1). No significant differences were seen between cases and matched pre-pandemic controls for these features. However, increased intervillous fibrin was seen in 33% of cases (9 of 27) but in none of the controls (Figure 1; p = 0.036). We found no association between the presence of increased intervillous fibrin and clinical features, including the presence of COVID-19 symptoms, co-morbidities, mode of delivery, or BMI. Overall, our
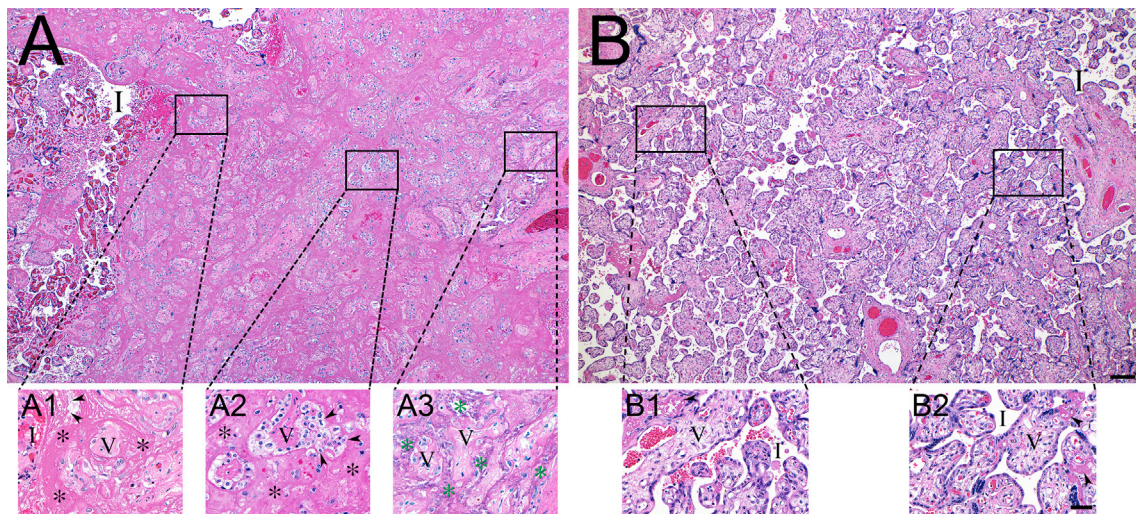
Figure 1. Histopathology of representative COVID-19 and matched control placentas

(A) COVID-19 placenta at low magnification revealed extensive intervillous fibrin deposition with only occasional areas of open (I) spaces.

(A1) High magnification of the edge of a blood-filled I space and the earliest fibrin deposition (asterisks). Trapped chorionic villi (V) have become avascular and fibrotic. Initial fibrillar fibrin (arrowheads) can be seen at the blood-fibrin interface.

(A2) Older area of I fibrin (asterisks) and trapped villi (V) revealing migration of trophoblasts (arrowheads) into the fibrin matrix.

(A3) The oldest area of I fibrin became calcified (green asterisks), encasing villous remnants (V).

(B) In sharp contrast, the control placenta revealed virtually no fibrin in the I space.

(B1 and B2) Representative magnified areas revealed normal villi (V) and open, maternal blood containing I space, with only occasional foci of fibrin formation (arrowheads).

Scale bars represents 200 µM for (A) and (B) and 50 µM for (A1)–(B2).

analysis suggests that increased intervillous fibrin may be the only distinct histologic feature observed in placentas from a subset of COVID-19-positive mothers.

Decreased ACE2 protein expression in the placenta over the course of normal pregnancy

We assessed the potential for SARS-CoV-2 infection of the placenta by examining placental expression of ACE2, the canonical receptor required for SARS-CoV-2 infection. Prior transcriptome studies have suggested that *ACE2* mRNA is absent or expressed at low levels in the placenta. Consistent with these previous reports, our analysis of bulk and single-cell RNA sequencing data in placentas from individuals with COVID-19 and control individuals demonstrates very low levels of *ACE2* gene expression at the term placenta (Figure S3). However, when protein-level ACE2 expression was examined by immunohistochemistry, we found ACE2 to be highly expressed in syncytiotrophoblast cells in first- and second-trimester placentas, with ACE2 protein expression virtually absent in normal-term placentas obtained from pre-pandemic control individuals (Figures 2B–2F).

Although the expression pattern of ACE2 in the placenta decreased steadily over gestational age in placentas derived from healthy pregnancies (Figure 2I), we found that ACE2 protein was present at significantly higher levels in term placentas collected from individuals with COVID-19 (Figure 2J). These findings suggest that detection of *ACE2* mRNA expression is not a reliable surrogate for ACE2 protein expression in the placenta and, importantly, that ACE2-mediated risk for placental infection by SARS-CoV-2 may vary over the course of pregnancy, with our detection of higher ACE2 levels in the first and second trimesters suggesting that the most vulnerability may exist prior to term. We detected minimal TMPRSS2 protein expression and no overlap of TMPRSS2 with ACE2 by immunohistochemistry in any term placentas.
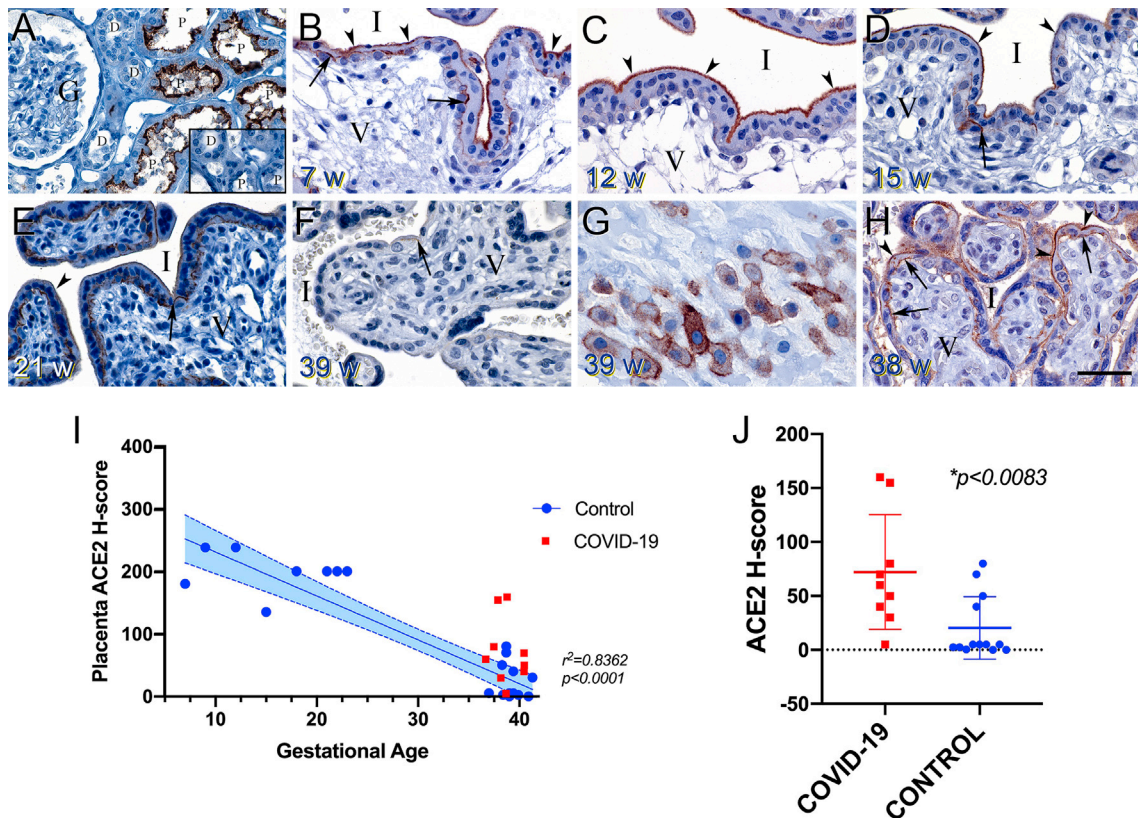
Figure 2. ACE2 protein expression in the placenta varies with gestational age

(A) Human kidney used as a positive control revealed strong apical staining of the proximal tubules (P). The distal tubules (D) and glomerulus (G) were negative. The inset shows a serial section of the same kidney stained with non-immune rabbit serum, resulting in no staining.

(B–D) Placentas derived from normal pregnancies between 7 and 15 weeks of gestation demonstrated strong, uniform, apical microvillus syncytiotrophoblast staining (arrowheads) and patchy strong basolateral staining at the cytotrophoblast-syncytiotrophoblast contact zone (arrows). V, villous core

(E) A normal 21-week placenta still exhibited syncytiotrophoblast surface staining (arrowhead) but to a lesser extent than the earlier samples. Cytotrophoblast-syncytiotrophoblast contact zone staining was still prominent (arrow).

(F) A representative normal placenta at 39 weeks revealed almost no ACE2 staining. Occasionally, staining at the cytotrophoblast-syncytiotrophoblast contact zone was noted (arrow).

(G) Normal extravillous invasive trophoblasts from a 39-week placenta demonstrated strong surface expression of ACE2 with variable cytoplasmic staining.

(H) Representative image of ACE2 expression in a 38-week placenta derived from an individual with symptomatic maternal COVID-19. Reappearance of strong apical microvillus syncytiotrophoblast (arrowheads) and cytotrophoblast-syncytiotrophoblast contact zone staining (arrows) was observed. All sections were cut at 5 µM, except (E), which was cut at 10 µM.

(A–H) Scale bars represent 50 µM.

(I) ACE2 H-score demonstrated steady loss of placental ACE2 with increasing gestational age in healthy pregnancies (p < 0.001). Linear regression (blue line) was fit to data from healthy controls (circles). 95% confidence interval is shown with dashed lines. Placentas derived from individuals with COVID-19 are depicted as red squares.

(J) ACE2 H-score was increased significantly in term placentas from individuals with COVID-19 (squares) compared with uninfected, matched control individuals (circles).

In vitro infection of primary isolated cytotrophoblasts with SARS-CoV-2

To determine whether the low rate of placental infection we observed in our case series was due to intrinsic resistance to SARS-CoV-2 infection by placental cells, we performed *in vitro* infection of placental cells to determine the infectious potential of SARS-CoV-2 at the placenta. We infected primary placental cells isolated from healthy term deliveries with a replication-competent infectious clone of SARS-CoV-2 expressing the fluorescent reporter mNeonGreen (icSARS-CoV-2-mNG)[20] for 24 h.
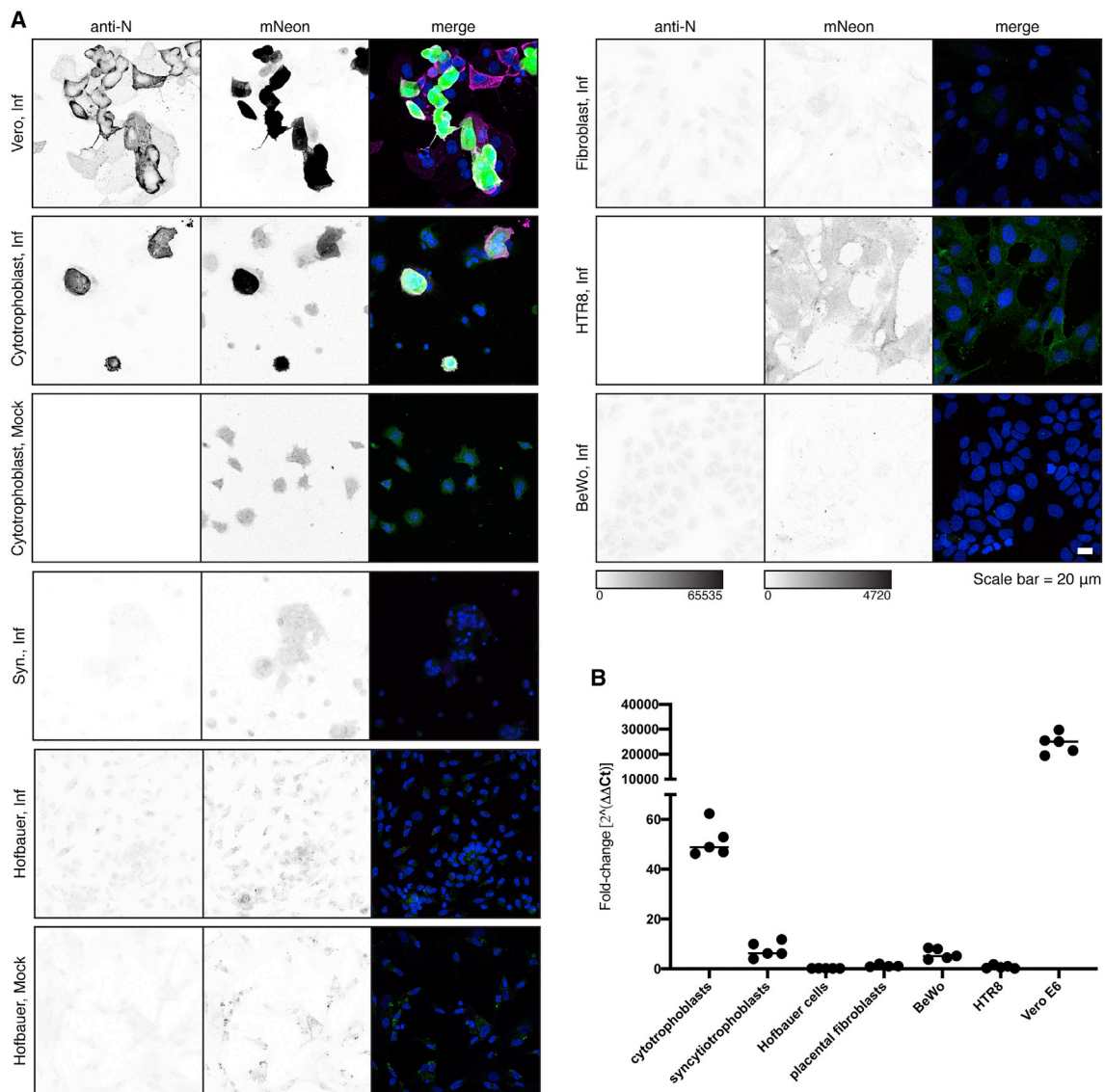
Figure 3. SARS-CoV-2 infection of placental cells *in vitro*

(A) Representative images of icSARS-CoV-2-mNG infection of primary placental cells, immortalized placental cell lines, and Vero E6 cells as measured by mNG expression and immunofluorescence staining of SARS-CoV-2 nucleocapsid (N). Images are displayed as maximum intensity projections of z stacks, and grayscale bars indicate measured fluorescence intensity in arbitrary digital units.

(B) Fold change quantification of SARS-CoV-2 N1 by qRT-PCR 24 h after infection. Cells were infected at an MOI of 5 for 1 h and washed three times with PBS before addition of fresh medium. Cells were washed and collected 24 h after infection. Data presented are representative results from one of three replicates.

We observed no detectable infection of Hofbauer cells or primary placental fibroblasts 24 h after infection (Figures 3A and 3B) or at 48, 72, and 96 h after infection. However, we found infection of primary isolated cytotrophoblasts, as observed by mNG reporter detection and staining for SARS-CoV-2 nucleocapsid (N) (Figure 3A). These findings were also consistent with SARS-CoV-2 N1 detection by qRT-PCR (Figure 3B). Primary isolated syncytiotrophoblasts (derived from cytotrophoblasts allowed to spontaneously differentiate for 72–96 h) were not as readily infected (Figures 3A and 3B), showing more limited capacity for infection even at 72 h after infection (Figure S4A). By immunofluorescence, only extremely rare individual cells

exhibiting viral mNG fluorescence and N staining (estimated to be less than 0.0001%) could be visualized. These infrequent positive cells were notably isolated cells excluded from the syncytialized regions of the culture, an appearance typical of cytotrophoblast cells defective for syncytialization (Figure S4B).

Immortalized cell lines are commonly used as a model for placental cell types. The BeWo line, a human choriocarcinoma line, is used to model villous cytotrophoblasts. The HTR-8/SVneo line is derived from invasive extravillous cytotrophoblasts isolated from first-trimester placentas and contains two cell populations.[21,22] Neither of these immortalized cell lines, BeWo or HTR-8/SVneo, exhibited significant infection with icSARS-CoV-2-mNG (Figure 3A). BeWo cells, however, similar to primary syncytiotrophoblasts, rarely (<0.0001%) exhibited viral mNG fluorescence co-localized with N staining. These results indicate that cytotrophoblasts are the placental cells most vulnerable to direct SARS-CoV-2 infection *in vitro*.

Transcriptional changes at the placenta during maternal COVID-19 reflect a localized inflammatory response to systemic SARS-CoV-2 infection

Despite the fact that cytotrophoblasts are permissive to SARS-CoV-2 infection *in vitro* and that SARS-COV-2 infection of syncytiotrophoblasts has been demonstrated in isolated cases,[12,18,23,24] SARS-CoV-2 infection was not detected in the majority of the placentas tested in our case series and in a recent cohort study of pregnant women with acute COVID-19.[25] This was true even in women with high NP viral loads and with symptomatic SARS-CoV-2 infection, including those with severe complications. This absence of placental infection suggested the presence of a localized and effective anti-viral response in the placenta. We thus used bulk RNA sequencing of placental villi to examine differences in placental gene expression between pregnant women with COVID-19 (n = 5) and uninfected control individuals matched for maternal age, gestational age, maternal comorbidities, and mode of delivery (n = 3).

In our comparison of the placental transcriptome in COVID-19 cases with matched controls, COVID-19 cases showed increased expression of genes associated with immune responses, suggesting a robust local response to respiratory infection even in the absence of localized placental infection (p < 0.05; Figure 4A). These changes in gene expression were largely shared among COVID-19 cases compared with controls, as indicated by their grouping upon hierarchical clustering; placental transcriptomes from COVID-19 cases largely clustered together and separately from healthy controls, with the exception of one case (COVID-2) (Figure 4A). Further analysis of differentially expressed genes by Gene Ontology indicated an enrichment in defense and immune response categories in COVID-19 cases compared with healthy controls (Figure 4B). The most significantly upregulated gene in the placenta during maternal SARS-CoV-2 infection was *HSPA1A*, which encodes the heat shock protein Hsp70 (Figure 4C), a proposed alarmin that has been implicated previously in placental vascular diseases and preeclampsia.[26–28] Among the top gene hits in the comparison of COVID-19 cases with controls were a significant number of immune genes and markers, including complement factors and interferon-stimulated genes (Figure S5).

Single-cell transcriptomic profiling of the placenta reveals a cell-type-specific immune response to maternal SARS-CoV-2 infection

We next assessed COVID-19-associated transcriptomic changes in the placenta in a cell-type-specific manner. To do so, we characterized placenta cells derived from placental villi and from the *decidua parietalis* from hospitalized individuals with
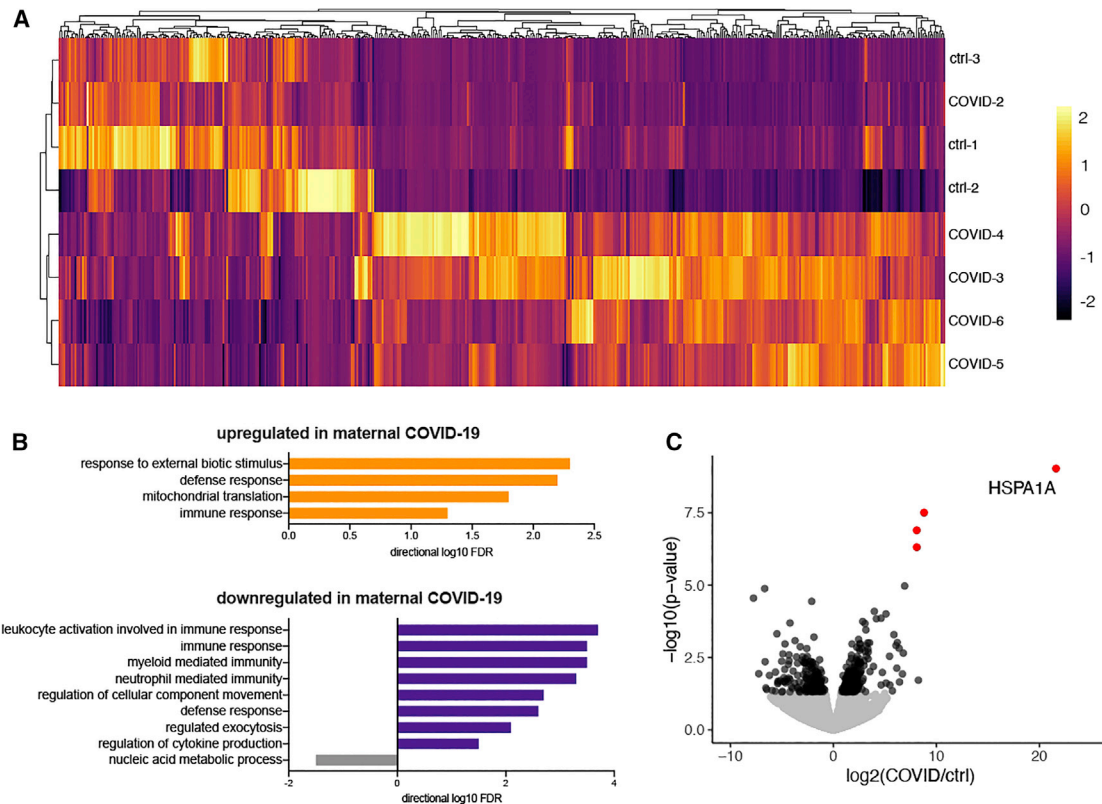
**Figure 4. HSPA1A is significantly upregulated in maternal COVID-19**

(A) Hierarchal clustering and heatmap of differentially expressed genes (p < 0.05). Bulk RNA sequencing (RNA-seq) was performed on placental villi isolated from control and maternal COVID cases.

(B) Gene Ontology of differentially expressed genes (p < 0.05) in bulk RNA-seq.

(C) Volcano plot indicating differentially expressed genes between control and maternal COVID-19 groups from bulk RNA-seq. Significant hits are depicted in red (p_{adj} < 0.05) and black (p < 0.05). Non-significant genes are shown in gray.

maternal acute COVID-19 (n = 2) and matched control individuals (n = 3) through unbiased, single-cell RNA sequencing. A total of 83,378 cells were included in the analysis, 44,140 from placental villi and 39,238 from the *decidua parietalis*. Placentas from these individuals with COVID-19 tested negative for SARS-CoV-2 by qRT-PCR. To further test for the presence of intracellular virus, open reading frames of SARS-CoV-2 (spike, ORF3a, envelope, membrane glycoprotein, ORF6, ORF7a, ORF8, nucleocapsid, and ORF10) were added to the reference genome before alignment with CellRanger. No viral transcripts were detected in any of the surveyed cells. We next performed unsupervised cluster analysis and represented single-cell transcriptome data from COVID-19 cases and controls in UMAP space (Figure 5A).

Classification of subsets at the maternal-fetal interface by single-cell RNA sequencing is challenging because of the presence of multiple cell types of maternal and fetal origin in highly active transcriptional states. We overcame this challenge by creating a reference set of cell-type-specific transcriptomes for cell types present at the human fetal-maternal interface, using cell-type-averaged expression values from three previously published placenta single-cell RNA sequencing studies.[29–31] We then compared single-cell transcriptomes in our dataset with this composite reference dataset, and, after annotating clusters by comparison with the reference dataset, we manually examined clusters for marker gene expression and annotated the
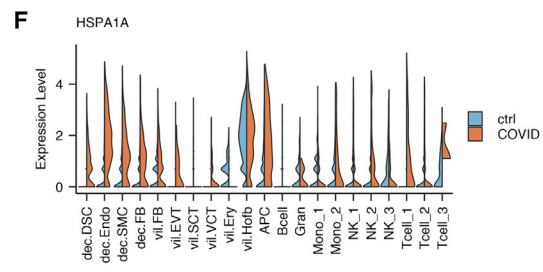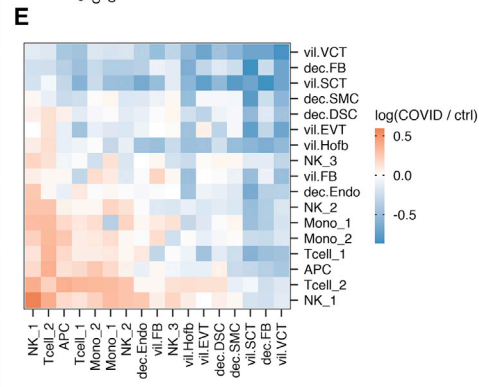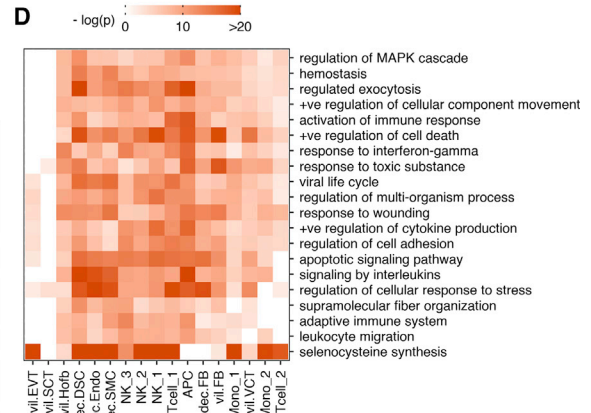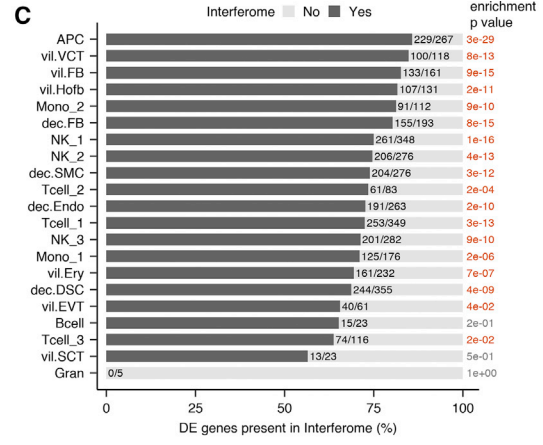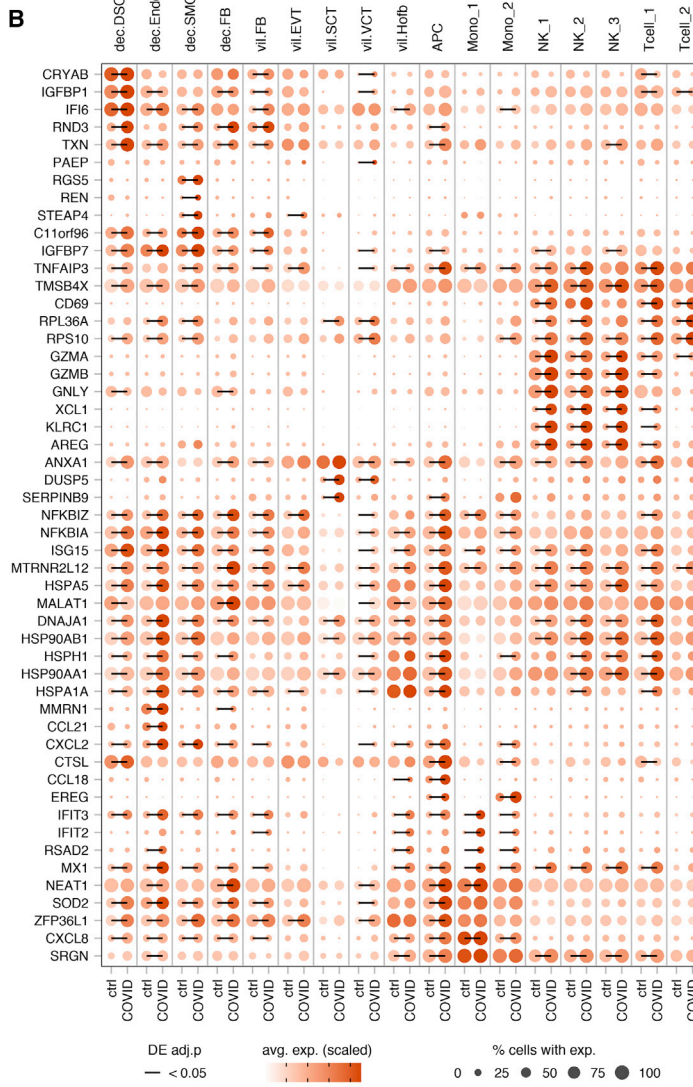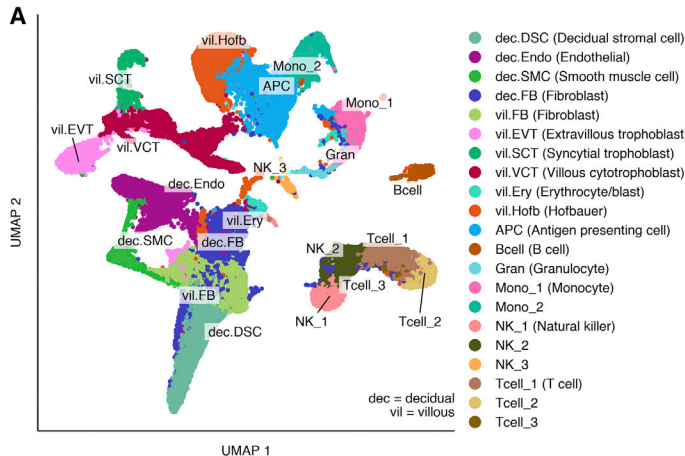
remaining clusters. With this approach, we identified 21 distinct cell types at the maternal-fetal interface (Figure 5A).

Differential gene expression analysis revealed significantly altered gene expression in immune and non-immune cell types in placentas from individuals with COVID-19 (Figure 5B), including markedly increased expression of pro-inflammatory genes and chemokines. In natural killer (NK) cells from pregnant women affected by COVID-19, we found significant enrichment of genes encoding cytotoxic proteins, including *GZMA*, *GZMB*, and *GNLY*, as well as a tissue repair growth factor, *AREG*. T cell subsets from COVID-19 cases showed upregulated *CD69*, a classical activation marker, as well as genes encoding ribosomal proteins, *RPL36A* and *RPS10*. Among endothelial cells, which have been implicated previously in COVID-19 pathogenesis, including COVID-19-associated thrombosis and vasculopathy,[34] we found evidence of increased innate immune responses in COVID-19 cases compared with controls, including significant upregulation of *ISG15*, an interferon-induced protein that has been implicated as a central player in host antiviral responses, and *NFKBIA* and *NFKBIZ*, critical regulators of the nuclear factor κB (NF-κB) pathway. Although we did not find significant expression of *ACE2* or *TMPRSS2* in placental and decidual cells in COVID-19 cases or healthy controls, we did find widespread expression of *CTSL*, an alternative SARS-CoV-2 entry co-receptor, in immune cells, fibroblasts, and trophoblasts at the maternal-fetal interface and increased *CTSL* expression in decidual stromal cells and decidual antigen-presenting cells in COVID-19.

Given the increasing evidence that hospitalized individuals with COVID-19 demonstrate strong type 1 interferon responses,[35,36] we used Interferome,[37] a database of interferon-regulated genes, to determine whether an interferon-driven inflammatory signature is displayed by the placenta. We find that cellular subsets at the maternal-fetal interface demonstrate significantly increased expression of interferon-related genes in individuals with COVID-19 compared with healthy control individuals (Figure 5C). Pathway analysis of all differentially expressed genes shows increased engagement of immune-related pathways in placental subsets from COVID-19 cases as well as increases in synthesis of selenocysteine associated with the anti-oxidative response to oxidative stress (Figure 5D). Finally, we wanted to find out whether the transcriptional changes observed in placental and decidual tissue suggested altered cellular interactions at the maternal-fetal interface during COVID-19 compared with healthy conditions. Using CellphoneDB signaling network analysis,[33] we found a significant increase in the number of interactions between immune cells at the maternal-fetal interface in COVID-19 cases compared with controls. Among the

Figure 5. Single-cell RNA-seq of placental cells demonstrates gene expression changes in placental immune cells during COVID-19

(A) UMAP projection of 83,378 single placenta cells from COVID-19 cases (n = 2 decidual and n = 2 villous samples) and uninfected controls (n = 2 decidual and n = 3 villous samples). Cell type annotations are based on correlation with reference datasets,[29–31] followed by manual examination of marker genes.

(B) Dotplot of the top 5 genes that are upregulated between COVID-19 and uninfected control samples for each annotated cell type based on fold difference. The size of the dots represents the percentage of cells in each cluster expressing the gene of interest; the intensity of the color reflects average scaled expression. Significantly altered expression between COVID-19 cases and controls (Bonferroni-adjusted, two-tailed Wilcoxon rank-sum test, p < 0.05) is marked by a solid black line.

(C) Interferome analysis demonstrating the fraction of differentially expressed genes in each cell type that are IFN responsive in COVID-19 cases compared with controls; p values for enrichment (observed over the expected fraction) were calculated using hypergeometric distribution.

(D) Clustered heatmap showing the top enriched functional terms according to Metascape[32] among differentially expressed genes between COVID-19 and control samples in the annotated placental cell types. Bars are colored to encode p values of increasing statistical significance.

(E) Heatmap depicting the log-transformed ratio (COVID-19 cases over controls) of number of ligand-receptor interactions between all placental cell type pairs, inferred using the CellphoneDB repository of ligands, receptors, and their interactions.[33] Red indicates cell type pairs with more interactions in COVID-19 cases compared with controls; blue indicates the opposite.

(F) Violin plots of *HSPA1A* expression at the placental villi and maternal decidua obtained by single-cell RNA-seq (scRNA-seq).

strongest enriched relationships identified in COVID-19 cases were the interactions of T cells with monocytes and NK cells (Figure 5E), suggesting innate-to-adaptive immune cell communication in the local placental environment during maternal COVID-19.

Consistent with the bulk RNA-seq data, analysis of single-cell data indicated significant upregulation of *HSPA1A*, the gene encoding Hsp70. HSPA1A was differentially expressed in select cellular subsets from individuals with COVID-19, including decidual antigen-presenting cells (APCs), decidual endothelial cells, and extravillous trophoblasts (Figure 5F).

DISCUSSION

Immune responses at the maternal-fetal interface can be a double-edged sword. These responses are critical for protecting the developing fetus from pathogen invasion, but, at the same time, placental inflammation itself may lead to pathological changes detrimental to pregnancy and fetal development.[38–41] In this study, we demonstrate that ACE2, the canonical entry receptor for SARS-CoV-2, is highly expressed during early gestation but exhibits low levels at full term in normal pregnancy; however, term placentas from COVID-19-affected individuals displayed increased ACE2 expression. Although primary trophoblast cells of the placenta are susceptible to SARS-CoV-2 infection *ex vivo*, SARS-CoV-2 RNA is rarely detected in the term placenta *in vivo*. Through bulk and single-cell RNA sequencing, we find evidence of robust immunological defenses mounted at the placenta in women with SARS-CoV-2 infection, even in the absence of viral RNA at the placenta. These findings suggest that placental immune responses during maternal respiratory SARS-CoV-2 infection may contribute to the poor pregnancy outcomes in COVID-19 and that active infection at the maternal-fetal interface is not required for immune activation at this distant site.

Although previous studies analyzing transcriptomic data have yielded mixed results regarding placental *ACE2* expression,[13–17] our immunohistochemical analysis conclusively demonstrated that ACE2 protein is present in the placenta despite low transcript levels. Recent studies of central nervous system and other tissue confirm that the mRNA level of *ACE2* is not a reliable surrogate for ACE2 protein expression.[17,42] ACE2 protein expression is highest in the first trimester and decreases over the course of a healthy pregnancy, indicating potential vulnerability to SARS-CoV-2 infection during early pregnancy. These data are supported by a recent study that reports decreasing *ACE2* mRNA levels with increasing gestational age.[43] Surprisingly, we found that ACE2 expression appears to be widely expressed in the placenta of individuals with COVID-19 at term despite low levels of ACE2 in the placentas of healthy control individuals at term. The unique modifying factors that drive placental ACE2 expression during COVID-19 remain unknown; however, studies of ACE2 expression during other disease states, including COPD, suggest that ACE2 is upregulated under inflammatory conditions.[44] Our data suggest that the hyperinflammatory state associated with COVID-19 may similarly increase ACE2 expression at the term placenta.

Although we find low mRNA expression of *ACE2* and *TMPRSS2*, we find high expression of a number of other proposed alternative SARS-CoV-2 receptors and co-factors, including *CTSL*, the gene encoding the Cathepsin L protease. CSTL regulates SARS-CoV-2 infection[45,46] and, in a genome-wide CRISPR screen of SARS-CoV-2 entry factors, was a top hit over TMPRSS2, second only to ACE2.[47] Although one of

many proposed entry factors, this finding suggests that there are other gene candidates that may promote entry of SARS-CoV-2 into the placenta.

Given the extremely low rate of placental infection by SARS-CoV-2 observed clinically, it was unknown whether the healthy term placenta is intrinsically susceptible to SARS-CoV-2. Prior case reports of SARS-CoV-2 infection of the placenta presented in the context of severe comorbid conditions and preeclampsia, suggesting that these placentas may have been uniquely capable of supporting infection. By isolating primary placental cells from elective cesarean sections without any comorbidities, complications, or evidence of infection, we show, through *in vitro* experiments, that trophoblasts from the healthy term placenta are capable of being infected by SARS-CoV-2.

The presence of ACE2 at the syncytiotrophoblast layer of the placental villi is consistent with the finding that the *in vivo* distribution of SARS-CoV-2 in rare cases of placental infection is intensely concentrated at the syncytiotrophoblast layer.[12,18,23,24] *In vitro*, however, we detected only minimal infection of primary syncytiotrophoblast cultures 72 h after infection, and intriguingly, this was visualized most robustly only in isolated, unsyncytialized cells. Cytotrophoblasts were the only placental cell type that we found to be reliably infected by SARS-CoV-2 *in vitro*. Given that syncytiotrophoblasts originate from spontaneous differentiation and fusion of cytotrophoblast stem cells,[48] it is possible that, removed from their *in vivo* context, these terminally differentiated cells are not as readily capable of supporting a productive viral infection *in vitro*. These findings may paint a clearer picture of the events leading to the pattern of placental infection observed *in vivo*; namely, that infected cytotrophoblasts could give rise to syncytiotrophoblasts that, through fusion, create a wall or layer of infected cells in the placenta. Alternatively, differences in susceptibility of primary placental cells to viral infection *in vivo* versus *in vitro* have also been demonstrated for Zika virus.[49] Zika virus has similarly been found to infect cytotrophoblasts[50] but not syncytiotrophoblasts because of constitutive interferon λ (IFN-λ) production[51]. Notably, unlike Zika virus and many other "TORCH" pathogens capable of causing congenital conditions following *in utero* exposure, SARS-CoV-2 does not appear to productively infect placental Hofbauer cells *in vivo* or *in* vitro.[52–54]

Despite the capacity of trophoblasts to be infected *in vitro*, SARS-CoV-2 invasion of the placenta has only been observed rarely *in vivo*. Indeed, despite active respiratory infections in our cohort, we detected SARS-CoV-2 RNA in the placenta in only one case of maternal COVID-19 at full term. However, it is important to note that we were only able to test placentas following parturition, with variable time between maternal symptom onset and delivery for each of our cases (Table 1). Thus, our study offers a view of the infectious status at only a snapshot in time and does not represent a generalizable view of the vulnerability of the placenta to SARS-CoV-2 infection prior to delivery. Low rates of placental infection may also be due to previously reported low levels of SARS-CoV-2 viremia[55] (i.e., the absence of a direct route of infection to the placenta *in vivo*), variable ACE2 expression at term, and/or protective immune responses elicited in the placenta. Unfortunately, we were unable to screen for potential maternal SARS-CoV-2 viremia in our group, but other studies found no detectable viremia in a large cohort of pregnant women[25] and an extremely low rate of detectable viremia in non-pregnant SARS-CoV-2-infected individuals (~1%).[56]

We find that the term placenta exhibits an inflammatory profile in the context of maternal upper respiratory tract infection and that an active, concurrent infection

locally is not required. Even in the absence of placental viral RNA, we observed localized gene expression differences in SARS-CoV-2-affected term placental and decidual tissue, indicating a marked immune response to maternal respiratory infection distinctly manifesting at the maternal-fetal interface. Gene Ontology analyses reveal certain immune pathways with increased expression and others with decreased expression in the placenta in response to maternal respiratory SARS-CoV-2 infection. Viral infection and immune activation likely perturb the maternal-fetal environment by upregulating pathways developed for pathogen response while downregulating the physiological immune pathways intricately involved in supporting normal pregnancy. The majority of these differentially expressed genes are IFN-regulated genes, demonstrating the capacity of the placenta to sense and respond to even distal infection.

Our cell-cell interaction analysis of transcriptomic changes observed at the maternal-fetal interface uncovered novel interactions, including between NK cells and T cells, that are features of the gene expression changes in placentas from COVID-19-infected women but not in uninfected control individuals. Decidual NK cells predominate at the maternal-fetal interface early in pregnancy, where they promote trophoblast invasion of the decidua and vascular remodeling, but decline to their lowest numbers at term. NK cells are known to play a distinct role in controlling human cytomegalovirus infection at the maternal-fetal interface,[57] but it is unknown whether they play a role in responding to non-TORCH infection.[58] Their activation is associated with release of cytokines and proangiogenic factors,[59] and dysregulation of these NK populations is associated with poor outcomes, such as preeclampsia,[60–63] We hypothesize that inappropriate activation of NK cells late in pregnancy may contribute to increased risk for complications in COVID-affected pregnant women. This hypothesis is further supported by the bulk sequencing data, in which top gene hits included genes involved in shaping NK and T cell tolerance at the maternal-fetal interface, such as HLA-C.[64]

Increased intervillous fibrin deposition in the placenta was observed in approximately one third of the COVID-19 cases. Intervillous fibrin is a pathological finding that increases with decreased maternal perfusion, increased maternal coagulability, and decreased thrombolytic function of trophoblasts.[65] Intervillous fibrin has been reported previously in cases of maternal COVID-19,[12,66] but the significance of this finding is unclear. SARS-CoV-2 infection is associated with endothelitis in other organ systems, including the brain and heart.[67–69] We hypothesize that maternal SARS-CoV-2 infection may likewise activate the maternal endothelium; this endothelitis may lead to impaired fibrinolysis, which, in turn, leads to excess fibrin deposition in a manner similar to that observed in preeclampsia.[70] Alternatively, or in addition, activation of immune cells at the maternal-fetal interface and circulating pro-inflammatory cytokines may trigger pro-coagulant signals in the local environment,[71] inducing tissue factor synthesis from syncytiotrophoblasts,[72] ultimately leading to accumulation of fibrin. Our single-cell transcriptomic analysis supports this hypothesis by demonstrating increased NK cell and endothelial cell expression of genes involved in supramolecular fiber organization pathways in placental and decidual tissue derived from individuals with COVID-19. Fibrin status may also be linked to other signs of oxidative stress in placentas affected by COVID-19. Bulk and single-cell sequencing analyses revealed differential expression of selenocysteine synthesis pathways that have been associated previously with oxidative damage and injury at the placenta. These changes have also been implicated in pregnancy-related conditions, including pre-eclampsia and pre-term labor, by altering the local redox balance and potential modulation of regional inflammatory responses.[73–75]

We found that *HSPA1A* (Hsp70) is highly upregulated at the maternal-fetal interface during maternal COVID-19. Notably, Hsp70 has been proposed as a potential alarmin that has been shown *in vitro* to stimulate proinflammatory processes associated with parturition and pre-term birth.[26,76,77] Hsp70 is associated with endothelial activation in placental vascular disease,[28] and serum levels are increased in cases of preeclampsia.[27,78,79] Extracellular Hsp70 is known to stimulate proinflammatory cytokines such as tumor necrosis factor alpha (TNF-α), interleukin-1β (IL-1β), and IL-6.[27] Hsp70 levels are significantly elevated in individuals exhibiting hemolysis, elevated liver enzymes, and low platelet count (HELLP syndrome) compared with individuals with severe preeclampsia without HELLP syndrome.[27,80] Intriguingly, there have been multiple reports of HELLP or HELLP-like syndrome in pregnant women affected by SARS-CoV-2 infection and COVID-19.[12,81,82] Although the interplay between COVID-19 and HELLP-like syndrome remains incompletely understood, these results suggest a potential common pathway for COVID-19-associated maternal morbidity and placental vascular diseases, including HELLP and preeclampsia.

By characterizing changes at the maternal-fetal interface in the context of systemic infection, our study indicates that maternal respiratory SARS-CoV-2 infection at term is associated with an inflammatory state in the placenta that may contribute to poor pregnancy outcomes in COVID-19. These immune responses at the maternal-fetal interface may serve to protect the placenta and fetus from infection, but they also have the potential to drive pathological changes with adverse consequences for developing embryos and fetuses because *in utero* inflammation is associated with multisystemic defects and developmental disorders in affected offspring.[40,83] Mouse models of congenital viral infection have also shown that type I IFN signaling during early embryonic development can cause fetal demise[84] through upregulation of IFITM proteins that interfere with cytotrophoblast fusion.[85,86] Further studies are therefore needed to assess the long-term consequences of SARS-CoV-2-associated immune activation in pregnant women regardless of the local infection status of the placenta.

Limitations of study

Participants in this study did not undergo routine, prospective SARS-CoV-2 screening by NP swab throughout the entirety of the pregnancy; thus, the exact onset of respiratory infection relative to the time of delivery and subsequent placental testing is unknown. Because we also cannot assess placental infection status throughout gestation, the low rate of PCR-positive placentas observed in this cohort does not definitively exclude the possibility of an earlier placental infection that resolved prior to delivery and testing. Our analysis is limited in that we only assessed placentas from women who were infected with SARS-CoV-2 at the time of or in the month prior to delivery and, thus, does not account for pathological and inflammatory changes at the placenta that result from infection during the first or second trimester. Indeed, our results demonstrating widespread ACE2 expression in the placenta during the first and second trimesters indicate that early pregnancy may be the most vulnerable time for SARS-CoV-2-induced placental pathology, and additional studies are needed to assess potential placental and fetal abnormalities associated with infection during early pregnancy.

STAR★METHODS

Detailed methods are provided in the online version of this paper and include the following:

- KEY RESOURCES TABLE

- RESOURCE AVAILABILITY
    - ○ Lead contact
    - ○ Materials availability
    - ○ Data and code availability
- EXPERIMENTAL MODEL AND SUBJECT DETAILS
    - ○ Human subjects
    - ○ Primary cell cultures
    - ○ Cell lines
- METHOD DETAILS
    - ○ SARS-CoV-2 detection in placenta by RT-qPCR
    - ○ SARS-CoV-2 S1 spike protein IgM and IgG serology testing
    - ○ Histopathological analysis of placenta
    - ○ ACE2 immunohistochemistry
    - ○ Primary cell isolations from placentas
    - ○ SARS-CoV-2 infections *in vitro*
    - ○ Immunofluorescence sample preparation and imaging
    - ○ Preparation of decidua and placental villi for bulk and single-cell sequencing
    - ○ Bulk RNA sequencing
    - ○ Single-cell RNA sequencing
- QUANTIFICATION AND STATISTICAL ANALYSIS

SUPPLEMENTAL INFORMATION

Supplemental information can be found online at https://doi.org/10.1016/j.medj.2021.04.016.

CONSORTIA

The members of the Yale IMPACT Team are Charles Dela Cruz, Allison Nelson, Anne L. Wyllie, Melissa Campbell, Elizabeth B. White, Rebecca Earnest, Sarah Lapidus, Joseph Lim, Maura Nakahata, Angela Nunez, Denise Shepard, Irene Matos, Yvette Strong, Kelly Anastasio, Kristina Brower, Maxine Kuang, Camila Odio, Bertie Geng, Maksym Minasyan, Melissa Linehan, Anjelica Martin, Tyler Rice, William Khoury-Hanold, Jessica Nouws, David McDonald, Kadi-Ann Rose, Yiyun Cao, Lokesh Sharma, Mikhail Smolgovsky, Abeer Obaid, Giuseppe Deluliis, Hong-Jai Park, Nicole Sonnert, Sofia Velazquez, Xiaohua Peng, Michael H. Askenase, Codruta Todeasa, Molly L. Bucklin, Maria Batsu, Adam J. Moore, and Eric Y. Wang.

AUTHOR CONTRIBUTIONS

A.L.-C. contributed to the design and implementation of the research, execution of experiments, analysis of the results, and writing of the manuscript. A.R.C. analyzed single-cell RNA sequencing and edited the manuscript. P.V. identified and obtained consent from affected and control individuals, collected biospecimens, and analyzed clinical and demographic information. L.I. and R.M. performed histological analyses. E.M.C., H.J.L., and K.M.N. contributed to *in vitro* studies. K.M.M. assisted with IHC experiments. Z.T. and S.G. performed placental cell isolation. S.D.P. and W.J.L.-C. contributed to bulk RNA sequencing analyses. E.S. contributed to single-cell RNA sequencing experiments and analysis. C.B.F.V. and N.D.G. performed and analyzed qRT-PCR of placental tissue. F.L. and A.R. performed plasma antibody assays. K.H.C., S.B., J.M.T., W.S., J.F., M.C.M., and L.K. assisted with case identification and biospecimen collection. A.C.-M. assisted with biospecimen collection and processing. A.I.K. contributed to study design and edited the manuscript. H.J.K. performed and analyzed IHC experiments, contributed to histological analyses and interpretation of results, and edited the manuscript. A.I. and S.F.F. designed and supervised the study.

DECLARATION OF INTERESTS

REFERENCES

1. Zambrano, L.D., Ellington, S., Strid, P., Galang, R.R., Oduyebo, T., Tong, V.T., Woodworth, K.R., Nahabedian, J.F., 3rd, Azziz-Baumgartner, E., Gilboa, S.M., and Meaney-Delman, D.; CDC COVID-19 Response Pregnancy and Infant Linked Outcomes Team (2020). Update: Characteristics of Symptomatic Women of Reproductive Age with Laboratory-Confirmed SARS-CoV-2 Infection by Pregnancy Status - United States, January 22-October 3, 2020. MMWR Morb. Mortal. Wkly. Rep. 69, 1641–1647.

2. Ahlberg, M., Neovius, M., Saltvedt, S., Söderling, J., Pettersson, K., Brandkvist, C., and Stephansson, O. (2020). Association of SARS-CoV-2 Test Status and Pregnancy Outcomes. JAMA 324, 1782–1785.

3. Abasse, S., Essabar, L., Costin, T., Mahisatra, V., Kaci, M., Braconnier, A., Serhal, R., Collet, L., and Fayssoil, A. (2020). Neonatal COVID-19 Pneumonia: Report of the First Case in a Preterm Neonate in Mayotte, an Overseas Department of France. Children (Basel) 7, E87.

4. Zimmermann, P., and Curtis, N. (2020). COVID-19 in Children, Pregnancy and Neonates: A Review of Epidemiologic and Clinical Features. Pediatr. Infect. Dis. J. 39, 469–477.

5. Sherer, M.L., Lei, J., Creisher, P., Jang, M., Reddy, R., Voegtline, K., Olson, S., Littlefield, K., Park, H.-S., Ursin, R.L., et al. (2020). Dysregulated immunity in SARS-CoV-2 infected pregnant women. medRxiv. https://doi.org/10.1101/2020.11.13.20231373.

6. Prochaska, E., Jang, M., and Burd, I. (2020). COVID-19 in pregnancy: Placental and neonatal involvement. Am. J. Reprod. Immunol. 84, e13306.

7. Barthold, S.W., Beck, D.S., and Smith, A.L. (1988). Mouse hepatitis virus and host determinants of vertical transmission and maternally-derived passive immunity in mice. Arch. Virol. 100, 171–183.

8. Cardenas, I., Means, R.E., Aldo, P., Koga, K., Lang, S.M., Booth, C.J., Manzur, A., Oyarzun, E., Romero, R., and Mor, G. (2010). Viral infection of the placenta leads to fetal inflammation and sensitization to bacterial products predisposing to preterm labor. J. Immunol. 185, 1248–1257.

9. Ng, W.F., Wong, S.F., Lam, A., Mak, Y.F., Yao, H., Lee, K.C., Chow, K.M., Yu, W.C., and Ho, L.C. (2006). The placentas of patients with severe acute respiratory syndrome: a pathophysiological evaluation. Pathology 38, 210–218.

10. Baud, D., Greub, G., Favre, G., Gengler, C., Jaton, K., Dubruc, E., and Pomar, L. (2020). Second-Trimester Miscarriage in a Pregnant Woman With SARS-CoV-2 Infection. JAMA 323, 2198–2200.

11. Hecht, J.L., Quade, B., Deshpande, V., Mino-Kenudson, M., Ting, D.T., Desai, N., Dygulska, B., Heyman, T., Salafia, C., Shen, D., et al. (2020). SARS-CoV-2 can infect the placenta and is not associated with specific placental histopathology: a series of 19 placentas from COVID-19-positive mothers. Mod. Pathol. 33, 2092–2103.

12. Hosier, H., Farhadian, S.F., Morotti, R.A., Deshmukh, U., Lu-Culligan, A., Campbell, K.H., Yasumoto, Y., Vogels, C.B., Casanovas-Massana, A., Vijayakumar, P., et al. (2020). SARS-CoV-2 infection of the placenta. J. Clin. Invest. 130, 4947–4953.

13. Pique-Regi, R., Romero, R., Tarca, A.L., Luca, F., Xu, Y., Alazizi, A., Leng, Y., Hsu, C.D., and Gomez-Lopez, N. (2020). Does the human placenta express the canonical cell entry mediators for SARS-CoV-2? eLife 9, e58716.

14. Li, M., Chen, L., Zhang, J., Xiong, C., and Li, X. (2020). The SARS-CoV-2 receptor ACE2 expression of maternal-fetal interface and fetal organs by single-cell transcriptome study. PLoS ONE *15*, e0230295.

15. Ashary, N., Bhide, A., Chakraborty, P., Colaco, S., Mishra, A., Chhabria, K., Jolly, M.K., and Modi, D. (2020). Single-Cell RNA-seq Identifies Cell Subsets in Human Placenta That Highly Expresses Factors Driving Pathogenesis of SARS-CoV-2. Front. Cell Dev. Biol. *8*, 783.

16. Singh, M., Bansal, V., and Feschotte, C. (2020). A Single-Cell RNA Expression Map of Human Coronavirus Entry Factors. Cell Rep. *32*, 108175.

17. Hikmet, F., Méar, L., Edvinsson, Å., Micke, P., Uhlén, M., and Lindskog, C. (2020). The protein expression profile of ACE2 in human tissues. Mol. Syst. Biol. *16*, e9610.

18. Patanè, L., Morotti, D., Giunta, M.R., Sigismondi, C., Piccoli, M.G., Frigerio, L., Mangili, G., Arosio, M., and Cornolti, G. (2020). Vertical transmission of coronavirus disease 2019: severe acute respiratory syndrome coronavirus 2 RNA on the fetal side of the placenta in pregnancies with coronavirus disease 2019-positive mothers and neonates at birth. Am. J. Obstet. Gynecol. MFM *2*, 100145.

19. Vivanti, A.J., Vauloup-Fellous, C., Prevot, S., Zupan, V., Suffee, C., Do Cao, J., Benachi, A., and De Luca, D. (2020). Transplacental transmission of SARS-CoV-2 infection. Nat. Commun. *11*, 3572.

20. Xie, X., Muruato, A., Lokugamage, K.G., Narayanan, K., Zhang, X., Zou, J., Liu, J., Schindewolf, C., Bopp, N.E., Aguilar, P.V., et al. (2020). An Infectious cDNA Clone of SARS-CoV-2. Cell Host Microbe *27*, 841–848.e3.

21. Graham, C.H., Hawley, T.S., Hawley, R.G., MacDougall, J.R., Kerbel, R.S., Khoo, N., and Lala, P.K. (1993). Establishment and characterization of first trimester human trophoblast cells with extended lifespan. Exp. Cell Res. *206*, 204–211.

22. Abou-Kheir, W., Barrak, J., Hadadeh, O., and Daoud, G. (2017). HTR-8/SVneo cell line contains a mixed population of cells. Placenta *50*, 1–7.

23. Taglauer, E., Benarroch, Y., Rop, K., Barnett, E., Sabharwal, V., Yarrington, C., and Wachman, E.M. (2020). Consistent localization of SARS-CoV-2 spike glycoprotein and ACE2 over TMPRSS2 predominance in placental villi of 15 COVID-19 positive maternal-fetal dyads. Placenta *100*, 69–74.

24. Facchetti, F., Bugatti, M., Drera, E., Tripodo, C., Sartori, E., Cancila, V., Papaccio, M., Castellani, R., Casola, S., Boniotti, M.B., et al. (2020). SARS-CoV2 vertical transmission with adverse effects on the newborn revealed through integrated immunohistochemical, electron microscopy and molecular analyses of Placenta. EBioMedicine *59*, 102951.

25. Edlow, A.G., Li, J.Z., Collier, A.Y., Atyeo, C., James, K.E., Boatin, A.A., Gray, K.J., Bordt, E.A., Shook, L.L., Yonker, L.M., et al. (2020). Assessment of Maternal and Neonatal SARS-CoV-2 Viral Load, Transplacental Antibody Transfer, and Placental Pathology in Pregnancies During the COVID-19 Pandemic. JAMA Netw. Open *3*, e2030455.

26. Brien, M.E., Baker, B., Duval, C., Gaudreault, V., Jones, R.L., and Girard, S. (2019). Alarmins at the maternal-fetal interface: involvement of inflammation in placental dysfunction and pregnancy complications. Can. J. Physiol. Pharmacol. *97*, 206–212.

27. Molvarec, A., Tamási, L., Losonczy, G., Madách, K., Prohászka, Z., and Rigó, J., Jr. (2010). Circulating heat shock protein 70 (HSPA1A) in normal and pathological pregnancies. Cell Stress Chaperones *15*, 237–247.

28. Liu, Y., Li, N., You, L., Liu, X., Li, H., and Wang, X. (2008). HSP70 is associated with endothelial activation in placental vascular diseases. Mol. Med. *14*, 561–566.

29. Vento-Tormo, R., Efremova, M., Botting, R.A., Turco, M.Y., Vento-Tormo, M., Meyer, K.B., Park, J.E., Stephenson, E., Polański, K., Goncalves, A., et al. (2018). Single-cell reconstruction of the early maternal-fetal interface in humans. Nature *563*, 347–353.

30. Pavličev, M., Wagner, G.P., Chavan, A.R., Owens, K., Maziarz, J., Dunn-Fletcher, C., Kallapur, S.G., Muglia, L., and Jones, H. (2017). Single-cell transcriptomics of the human placenta: inferring the cell communication network of the maternal-fetal interface. Genome Res. *27*, 349–361.

31. Suryawanshi, H., Morozov, P., Straus, A., Sahasrabudhe, N., Max, K.E.A., Garzia, A., Kustagi, M., Tuschl, T., and Williams, Z. (2018). A single-cell survey of the human first-trimester placenta and decidua. Sci. Adv. *4*, eaau4788.

32. Zhou, Y., Zhou, B., Pache, L., Chang, M., Khodabakhshi, A.H., Tanaseichuk, O., Benner, C., and Chanda, S.K. (2019). Metascape provides a biologist-oriented resource for the analysis of systems-level datasets. Nat. Commun. *10*, 1523.

33. Efremova, M., Vento-Tormo, M., Teichmann, S.A., and Vento-Tormo, R. (2020). CellPhoneDB: inferring cell-cell communication from combined expression of multi-subunit ligand-receptor complexes. Nat. Protoc. *15*, 1484–1506.

34. Goshua, G., Pine, A.B., Meizlish, M.L., Chang, C.H., Zhang, H., Bahel, P., Baluha, A., Bar, N., Bona, R.D., Burns, A.J., et al. (2020). Endotheliopathy in COVID-19-associated coagulopathy: evidence from a single-centre, cross-sectional study. Lancet Haematol. *7*, e575–e582.

35. Acharya, D., Liu, G., and Gack, M.U. (2020). Dysregulation of type I interferon responses in COVID-19. Nat. Rev. Immunol. *20*, 397–398.

36. Lee, J.S., and Shin, E.C. (2020). The type I interferon response in COVID-19: implications for treatment. Nat. Rev. Immunol. *20*, 585–586.

37. Rusinova, I., Forster, S., Yu, S., Kannan, A., Masse, M., Cumming, H., Chapman, R., and Hertzog, P.J. (2013). Interferome v2.0: an updated database of annotated interferon-regulated genes. Nucleic Acids Res. *41*, D1040–D1046.

38. Nadeau-Vallée, M., Obari, D., Palacios, J., Brien, M.E., Duval, C., Chemtob, S., and Girard, S. (2016). Sterile inflammation and pregnancy complications: a review. Reproduction *152*, R277–R292.

39. Weckman, A.M., Ngai, M., Wright, J., McDonald, C.R., and Kain, K.C. (2019). The Impact of Infection in Pregnancy on Placental Vascular Development and Adverse Birth Outcomes. Front. Microbiol. *10*, 1924.

40. Lu-Culligan, A., and Iwasaki, A. (2020). The Role of Immune Factors in Shaping Fetal Neurodevelopment. Annu. Rev. Cell Dev. Biol. *36*, 441–468.

41. Yockey, L.J., Lucas, C., and Iwasaki, A. (2020). Contributions of maternal and fetal antiviral immunity in congenital disease. Science *368*, 608–612.

42. Song, E., Zhang, C., Israelow, B., Lu-Culligan, A., Prado, A.V., Skriabine, S., Lu, P., Weizman, O.-E., Liu, F., Dai, Y., et al. (2021). Neuroinvasion of SARS-CoV-2 in human and mouse brain. J. Exp. Med. *218*, e20202135.

43. Bloise, E., Zhang, J., Nakpu, J., Hamada, H., Dunk, C.E., Li, S., Imperio, G.E., Nadeem, L., Kibschull, M., Lye, P., et al. (2021). Expression of severe acute respiratory syndrome coronavirus 2 cell entry genes, angiotensin-converting enzyme 2 and transmembrane protease serine 2, in the placenta across gestation and at the maternal-fetal interface in pregnancies complicated by preterm birth or preeclampsia. Am. J. Obstet. Gynecol. *224*, 298.e1–298.e8.

44. Leung, J.M., Yang, C.X., Tam, A., Shaipanich, T., Hackett, T.L., Singhera, G.K., Dorscheid, D.R., and Sin, D.D. (2020). ACE-2 expression in the small airway epithelia of smokers and COPD patients: implications for COVID-19. Eur. Respir. J. *55*, 2000688.

45. Shang, J., Wan, Y., Luo, C., Ye, G., Geng, Q., Auerbach, A., and Li, F. (2020). Cell entry mechanisms of SARS-CoV-2. Proc. Natl. Acad. Sci. USA *117*, 11727–11734.

46. Ou, X., Liu, Y., Lei, X., Li, P., Mi, D., Ren, L., Guo, L., Guo, R., Chen, T., Hu, J., et al. (2020). Characterization of spike glycoprotein of SARS-CoV-2 on virus entry and its immune cross-reactivity with SARS-CoV. Nat. Commun. *11*, 1620.

47. Wei, J., Alfajaro, M.M., DeWeirdt, P.C., Hanna, R.E., Lu-Culligan, W.J., Cai, W.L., Strine, M.S., Zhang, S.M., Graziano, V.R., Schmitz, C.O., et al. (2021). Genome-wide CRISPR Screens Reveal Host Factors Critical for SARS-CoV-2 Infection. Cell *184*, 76–91.e13.

48. Kliman, H.J., Nestler, J.E., Sermasi, E., Sanger, J.M., and Strauss, J.F., 3rd (1986). Purification, characterization, and in vitro differentiation of cytotrophoblasts from human term placentae. Endocrinology *118*, 1567–1582.

49. Jurado, K.A., Simoni, M.K., Tang, Z., Uraki, R., Hwang, J., Householder, S., Wu, M., Lindenbach, B.D., Abrahams, V.M., Guller, S., and Fikrig, E. (2016). Zika virus productively infects primary human placenta-specific macrophages. JCI Insight *1*, e88461.

50. Tabata, T., Petitt, M., Puerta-Guardo, H., Michlmayr, D., Wang, C., Fang-Hoover, J., Harris, E., and Pereira, L. (2016). Zika Virus Targets Different Primary Human Placental Cells, Suggesting Two Routes for Vertical Transmission. Cell Host Microbe 20, 155–166.

51. Bayer, A., Lennemann, N.J., Ouyang, Y., Bramley, J.C., Morosky, S., Marques, E.T., Jr., Cherry, S., Sadovsky, Y., and Coyne, C.B. (2016). Type III Interferons Produced by Human Placental Trophoblasts Confer Protection against Zika Virus Infection. Cell Host Microbe 19, 705–712.

52. Reyes, L., and Golos, T.G. (2018). Hofbauer Cells: Their Role in Healthy and Complicated Pregnancy. Front. Immunol. 9, 2628.

53. Simoni, M.K., Jurado, K.A., Abrahams, V.M., Fikrig, E., and Guller, S. (2017). Zika virus infection of Hofbauer cells. Am. J. Reprod. Immunol. 77, https://doi.org/10.1111/aji.12613.

54. Coyne, C.B., and Lazear, H.M. (2016). Zika virus - reigniting the TORCH. Nat. Rev. Microbiol. 14, 707–715.

55. Kim, J.M., Kim, H.M., Lee, E.J., Jo, H.J., Yoon, Y., Lee, N.J., Son, J., Lee, Y.J., Kim, M.S., Lee, Y.P., et al. (2020). Detection and Isolation of SARS-CoV-2 in Serum, Urine, and Stool Specimens of COVID-19 Patients from the Republic of Korea. Osong Public Health Res. Perspect. 11, 112–117.

56. Wang, W., Xu, Y., Gao, R., Lu, R., Han, K., Wu, G., and Tan, W. (2020). Detection of SARS-CoV-2 in Different Types of Clinical Specimens. JAMA 323, 1843–1844.

57. de Mendonça Vieira, R., Meagher, A., Crespo, A.C., Kshirsagar, S.K., Iyer, V., Norwitz, E.R., Strominger, J.L., and Tilburgs, T. (2020). Human Term Pregnancy Decidual NK Cells Generate Distinct Cytotoxic Responses. J. Immunol. 204, 3149–3159.

58. Jabrane-Ferrat, N. (2019). Features of Human Decidual NK Cells in Healthy Pregnancy and During Viral Infection. Front. Immunol. 10, 1397.

59. Hanna, J., Goldman-Wohl, D., Hamani, Y., Avraham, I., Greenfield, C., Natanson-Yaron, S., Prus, D., Cohen-Daniel, L., Arnon, T.I., Manaster, I., et al. (2006). Decidual NK cells regulate key developmental processes at the human fetal-maternal interface. Nat. Med. 12, 1065–1074.

60. Fukui, A., Yokota, M., Funamizu, A., Nakamua, R., Fukuhara, R., Yamada, K., Kimura, H., Fukuyama, A., Kamoi, M., Tanaka, K., and Mizunuma, H. (2012). Changes of NK cells in preeclampsia. Am. J. Reprod. Immunol. 67, 278–286.

61. Taylor, E.B., and Sasser, J.M. (2017). Natural killer cells and T lymphocytes in pregnancy and pre-eclampsia. Clin. Sci. (Lond.) 131, 2911–2917.

62. Goldman-Wohl, D., and Yagel, S. (2008). NK cells and pre-eclampsia. Reprod. Biomed. Online 16, 227–231.

63. Cornelius, D.C., and Wallace, K. (2019). Decidual natural killer cells: A critical pregnancy mediator altered in preeclampsia. EBioMedicine 39, 31–32.

64. Papúchová, H., Meissner, T.B., Li, Q., Strominger, J.L., and Tilburgs, T. (2019). The Dual Role of HLA-C in Tolerance and Immunity at the Maternal-Fetal Interface. Front. Immunol. 10, 2730.

65. Fox, H. (1967). Perivillous fibrin deposition in the human placenta. Am. J. Obstet. Gynecol. 98, 245–251.

66. Shanes, E.D., Mithal, L.B., Otero, S., Azad, H.A., Miller, E.S., and Goldstein, J.A. (2020). Placental Pathology in COVID-19. Am. J. Clin. Pathol. 154, 23–32.

67. Libby, P., and Lüscher, T. (2020). COVID-19 is, in the end, an endothelial disease. Eur. Heart J. 41, 3038–3044.

68. Lee, M.-H., Perl, D.P., Nair, G., Li, W., Maric, D., Murray, H., Dodd, S.J., Koretsky, A.P., Watts, J.A., Cheung, V., et al. (2021). Microvascular Injury in the Brains of Patients with Covid-19. N. Engl. J. Med. 384, 481–483.

69. Jin, Y., Ji, W., Yang, H., Chen, S., Zhang, W., and Duan, G. (2020). Endothelial activation and dysfunction in COVID-19: from basic mechanisms to potential therapeutic approaches. Signal Transduct. Target. Ther. 5, 293.

70. Stalker, A.L. (1976). Fibrin deposition in pregnancy. J. Clin. Pathol. Suppl. (R Coll. Pathol.) 10, 70–76.

71. Li, M., and Huang, S.J. (2009). Innate immunity, coagulation and placenta-related adverse pregnancy outcomes. Thromb. Res. 124, 656–662.

72. Aharon, A., Brenner, B., Katz, T., Miyagi, Y., and Lanir, N. (2004). Tissue factor and tissue factor pathway inhibitor levels in trophoblast cells: implications for placental hemostasis. Thromb. Haemost. 92, 776–786.

73. Qazi, I.H., Angel, C., Yang, H., Pan, B., Zoidis, E., Zeng, C.-J., Han, H., and Zhou, G.-B. (2018). Selenium, Selenoproteins, and Female Reproduction: A Review. Molecules 23, 3053.

74. Khera, A., Dong, L.F., Holland, O., Vanderlelie, J., Pasdar, E.A., Neuzil, J., and Perkins, A.V. (2015). Selenium supplementation induces mitochondrial biogenesis in trophoblasts. Placenta 36, 863–869.

75. Mariath, A.B., Bergamaschi, D.P., Rondó, P.H., Tanaka, A.C., Hinnig, Pde.F., Abbade, J.F., and Diniz, S.G. (2011). The possible role of selenium status in adverse pregnancy outcomes. Br. J. Nutr. 105, 1418–1428.

76. Pockley, A.G. (2003). Heat shock proteins as regulators of the immune response. Lancet 362, 469–476.

77. Geng, J., Li, H., Huang, C., Chai, J., Zheng, R., Li, F., and Jiang, S. (2017). Functional analysis of HSPA1A and HSPA8 in parturition. Biochem. Biophys. Res. Commun. 483, 371–379.

78. Hromadnikova, I., Dvorakova, L., Kotlabova, K., Kestlerova, A., Hympanova, L., Novotna, V., Doucha, J., and Krofta, L. (2016). Circulating heat shock protein mRNA profile in gestational hypertension, pre-eclampsia & foetal growth restriction. Indian J. Med. Res. 144, 229–237.

79. Saghafi, N., Pourali, L., Ghavami Ghanbarabadi, V., Mirzamarjani, F., and Mirteimouri, M. (2018). Serum heat shock protein 70 in preeclampsia and normal pregnancy: A systematic review and meta-analysis. Int. J. Reprod. Biomed. (Yazd) 16, 1–8.

80. Molvarec, A., Rigó, J., Jr., Nagy, B., Walentin, S., Szalay, J., Füst, G., Karádi, I., and Prohászka, Z. (2007). Serum heat shock protein 70 levels are decreased in normal human pregnancy. J. Reprod. Immunol. 74, 163–169.

81. Figueras, F., LLurba, E., Martinez-Portilla, R., Mora, J., Crispi, F., and Gratacos, E. (2020). COVID-19 causing HELLP-like syndrome in pregnancy and role of angiogenic factors for differential diagnosis. medRxiv. https://doi.org/10.1101/2020.07.10.20133801.

82. Futterman, I., Toaff, M., Navi, L., and Clare, C.A. (2020). COVID-19 and HELLP: Overlapping Clinical Pictures in Two Gravid Patients. AJP Rep. 10, e179–e182.

83. Makinson, R., Lloyd, K., Grissom, N., and Reyes, T.M. (2019). Exposure to in utero inflammation increases locomotor activity, alters cognitive performance and drives vulnerability to cognitive performance deficits after acute immune activation. Brain Behav. Immun. 80, 56–65.

84. Yockey, L.J., Jurado, K.A., Arora, N., Millet, A., Rakib, T., Milano, K.M., Hastings, A.K., Fikrig, E., Kong, Y., Horvath, T.L., et al. (2018). Type I interferons instigate fetal demise after Zika virus infection. Sci. Immunol. 3, eaao1680.

85. Zani, A., Zhang, L., McMichael, T.M., Kenney, A.D., Chemudupati, M., Kwiek, J.J., Liu, S.L., and Yount, J.S. (2019). Interferon-induced transmembrane proteins inhibit cell fusion mediated by trophoblast syncytins. J. Biol. Chem. 294, 19844–19851.

86. Buchrieser, J., Degrelle, S.A., Couderc, T., Nevers, Q., Disson, O., Manet, C., Donahue, D.A., Porrot, F., Hillion, K.H., Perthame, E., et al. (2019). IFITM proteins inhibit placental syncytiotrophoblast formation and promote fetal demise. Science 365, 176–180.

87. Schneider, C.A., Rasband, W.S., and Eliceiri, K.W. (2012). NIH Image to ImageJ: 25 years of image analysis. Nat. Methods 9, 671–675.

88. Bray, N.L., Pimentel, H., Melsted, P., and Pachter, L. (2016). Near-optimal probabilistic RNA-seq quantification. Nat. Biotechnol. 34, 525–527.

89. Durinck, S., Spellman, P.T., Birney, E., and Huber, W. (2009). Mapping identifiers for the integration of genomic datasets with the R/Bioconductor package biomaRt. Nat. Protoc. 4, 1184–1191.

90. Soneson, C., Love, M.I., and Robinson, M.D. (2015). Differential analyses for RNA-seq: transcript-level estimates improve gene-level inferences. F1000Res. 4, 1521.

91. Love, M.I., Huber, W., and Anders, S. (2014). Moderated estimation of fold change and dispersion for RNA-seq data with DESeq2. Genome Biol. 15, 550.

92. Stuart, T., Butler, A., Hoffman, P., Hafemeister, C., Papalexi, E., Mauck, W.M.,

3rd, Hao, Y., Stoeckius, M., Smibert, P., and Satija, R. (2019). Comprehensive Integration of Single-Cell Data. Cell *177*, 1888–1902.e21, https://doi.org/10.1016/j.cell.2019.05.031.

93. Kliman, H.J., Sammar, M., Grimpel, Y.I., Lynch, S.K., Milano, K.M., Pick, E., Bejar, J., Arad, A., Lee, J.J., Meiri, H., and Gonen, R. (2012). Placental protein 13 and decidual zones of necrosis: an immunologic diversion that may be linked to preeclampsia. Reprod. Sci. *19*, 16–30.

94. Tang, Z., Tadesse, S., Norwitz, E., Mor, G., Abrahams, V.M., and Guller, S. (2011). Isolation of hofbauer cells from human term placentas with high yield and purity. Am. J. Reprod. Immunol. *66*, 336–348.

95. Vogels, C.B.F., Brito, A.F., Wyllie, A.L., Fauver, J.R., Ott, I.M., Kalinich, C.C., Petrone, M.E., Casanovas-Massana, A., Catherine Muenker, M., Moore, A.J., et al. (2020). Analytical sensitivity and efficiency comparisons of SARS-CoV-2 RT-qPCR primer-probe sets. Nat. Microbiol. *5*, 1299–1305.

96. Amanat, F., Nguyen, T., Chromikova, V., Strohmeier, S., Stadlbauer, D., Javier, A., Jiang, K., Asthagiri-Arunkumar, G., Polanco, J., Bermudez-Gonzalez, M., et al. (2020). A serological assay to detect SARS-CoV-2 seroconversion in humans. medRxiv. https://doi.org/10.1101/2020.03.17.20037713.

97. Khong, T.Y., Mooney, E.E., Ariel, I., Balmus, N.C., Boyd, T.K., Brundler, M.A., Derricott, H., Evans, M.J., Faye-Petersen, O.M., Gillan, J.E., et al. (2016). Sampling and Definitions of Placental Lesions: Amsterdam Placental Workshop Group Consensus Statement. Arch. Pathol. Lab. Med. *140*, 698–713.

98. Kliman, H.J., Quaratella, S.B., Setaro, A.C., Siegman, E.C., Subha, Z.T., Tal, R., Milano, K.M., and Steck, T.L. (2018). Pathway of Maternal Serotonin to the Human Embryo and Fetus. Endocrinology *159*, 1609–1629.

99. Thike, A.A., Chng, M.J., Fook-Chong, S., and Tan, P.H. (2001). Immunohistochemical expression of hormone receptors in invasive breast carcinoma: correlation of results of H-score with pathological parameters. Pathology *33*, 21–25.

100. Xu, Y., Plazyo, O., Romero, R., Hassan, S.S., and Gomez-Lopez, N. (2015). Isolation of Leukocytes from the Human Maternal-fetal Interface. J. Vis. Exp. e52863.

101. Team, R.C. (2020). R: A Language and Environment for Statistical Computing (R Foundation for Statistical Computing).

102. Hafemeister, C., and Satija, R. (2019). Normalization and variance stabilization of single-cell RNA-seq data using regularized negative binomial regression. Genome Biol. *20*, 296.

STAR★METHODS

KEY RESOURCES TABLE

REAGENT or RESOURCE	SOURCE	IDENTIFIER
Antibodies		
Anti-ACE2 antibody	Abcam	Cat#ab108252; RRID: AB_10864415
Anti-SARS-CoV-2 nucleocapsid antibody	GeneTex	Cat#GTX135357; RRID: AB_2868464
HRP anti-human IgG antibody	GenScript	Cat#A00166
Anti-human IgM (mu-chain specific)-peroxidase antibody	Sigma-Aldrich	Cat#A6907; RRID: AB_258318
Donkey anti-rabbit IgG, Alexa Fluor 594	Jackson ImmunoResearch	Cat#711-585-152; RRID: AB_2340621
Mouse monoclonal anti-CD9	Biolegend	Cat#312102; RRID: AB_314907
Mouse monoclonal anti-CD45	Biolegend	Cat#304002; RRID: AB_314390
Mouse monoclonal anti-EGFR	SCBT	Cat#sc-120; RRID: AB_627492
Mouse monoclonal anti-CD10	Biolegend	Cat#312202; RRID: AB_314913
Goat anti-mouse IgG (Fc) coated magnetic particles	Spherotech	Cat#MMFc-40-10
Normal rabbit serum	Sigma-Aldrich	Cat#R9133
MACH 2 rabbit HRP-polymer	Biocare Medical	Cat#RHRP520L
Bacterial and virus strains		
icSARS-CoV-2 mNG	Xie et al.[20]	N/A
Biological samples		
Term placental tissue	Yale New Haven Health	N/A
First and second trimester placental tissue	Bnai Zion Medical Center	N/A
Second trimester placental tissue	University of Pittsburgh Biospecimen Core	N/A
Chemicals, peptides, and recombinant proteins		
Recombinant SARS-CoV-2 S1 protein	ACROBiosystems	Cat#S1N-C52H3
Tween 20	Sigma-Aldrich	Cat#P1379
Tween 20	Sigma-Aldrich	Cat#P9416
Triton X-100	AmericanBio	Cat#AB02025
RNase A	QIAGEN	Cat#19101
TMB Substrate Reagent Set	BD Biosciences	Cat#555214
Sulfuric Acid Solution 10N	Thermo Fischer Scientific	Cat#SA200-1
2.5% Trypsin (10X)	Thermo Scientific	Cat#15090-046
DNase I	Roche	Cat#10104159001
Collagenase A	Roche	Cat#11088793001
Percoll	GE Healthcare	Cat#17-0891-01
10% Neutral buffered formalin	VWR	Cat#16004-126
Liberase TM	Roche	Cat#LIBTM-RO
Dnase I	Roche	Cat#10104159001
ACK lysing buffer	GIBCO	Cat#A1049201
Xylenes	Sigma-Aldrich	Cat#534056
Sodium citrate	Sigma-Aldrich	Cat#W302600
Hydrogen peroxide	Sigma-Aldrich	Cat#H1009
Hematoxylin QS	Vector Laboratories	Cat#H-3404
VectaMount mounting medium	Vector Laboratories	Cat#H-5000
Paraformaldehyde	Electron Microscopy Sciences	Cat#15710
Bovine serum albumin	Sigma-Aldrich	Cat#A9647
Bovine serum albumin	Sigma-Aldrich	Cat#A7906
1,4-Diazabicyclo[2.2.2]octane (DABCO)	Sigma-Aldrich	Cat#D27802
Trizol	Invitrogen	Cat#15596018
Critical commercial assays		
10x Chromium Single Cell 3¢ Library & Gel Bead Kit v3	10x Genomics	Cat#PN-1000075

(Continued on next page)

Continued

REAGENT or RESOURCE	SOURCE	IDENTIFIER
MagMAX Viral/Pathogen Nucleic Acid Isolation Kit	ThermoFisher Scientific	Cat#A48310
RNeasy Mini Kit	QIAGEN	Cat#74106
Luna Universal Probe One-Step RT-qPCR Kit	New England Biolabs	Cat#E3006E
Betazoid DAB Chromogen Kit	Biocare Medical	Cat#BDB2004
Deposited data		
Bulk RNA sequencing data	This study	GSE171995
Single cell RNA sequencing data	This study	GSE171381
Experimental models: Cell lines		
Vero-E6 cells	ATCC	Cat#CRL-1586
BeWo cells	ATCC	Cat#CCL-98
HTR-8/SVneo cells	Graham et al.;[21] ATCC	Cat#CRL-3271
Oligonucleotides		
nCOV_N1 forward primer GACCCCAAAATCAGCGAAAT	IDT	Cat#10006830
nCOV_N1 reverse primer TCT GGTTACTGCCAGTTGAATCTG	IDT	Cat#10006831
nCOV_N1 probe FAM-ACCCCG CATTACGTTTGGTGGACC-IBFQ	IDT	Cat#10006832
nCOV_N2 forward primer TTACAAACATTGGCCGCAAA	IDT	Cat#10006833
nCOV_N2 reverse primer GCGCGACATTCCGAAGAA	IDT	Cat#10006834
nCOV_N2 probe FAM-ACAATT TGCCCCCAGCGCTTCAG-IBFQ	IDT	Cat#10006835
RNase P forward primer AG ATTTGGACCTGCGAGCG	IDT	Cat#10006836
RNase P reverse primer GA GCGGCTGTCTCCACAAGT	IDT	Cat#10006837
RNase P probe FAM-TTCTGAC CTGAAGGCTCTGCGCG-IBFQ	IDT	Cat#10006838
Software and algorithms		
R	R Foundation	https://www.r-project.org/
Python	Python Software Foundation	https://www.python.org/
Prism 8 (v8.0.1)	GraphPad	https://www.graphpad.com/scientific-software/prism/
ImageJ	Schneider et al.[87]	https://imagej.net/Welcome
Kallisto (v0.46.1)	Bray et al.[88]	https://pachterlab.github.io/kallisto/download
biomaRt (v2.40.5)	Durinck et al.[89]	https://bioconductor.org/packages/release/bioc/html/biomaRt.html
Tximport (v1.12.3)	Soneson et al.[90]	https://bioconductor.org/packages/release/bioc/html/tximport.html
DESeq2 (v1.24.0)	Love et al.[91]	https://bioconductor.org/packages/release/bioc/html/DESeq2.html
Cell Ranger (v3.0.2)	10x Genomics	https://support.10xgenomics.com/single-cell-gene-expression/software/pipelines/latest/installation
Seurat (v3.2.2)	Stuart et al.[92]	https://satijalab.org/seurat/
Interferome (v2.01)	Rusinova et al.[37]	http://www.interferome.org/interferome/home.jspx
Metascape	Zhou et al.[32]	https://metascape.org/
CellPhoneDB (v2.1.4)	Efremova et al.[33]	https://www.cellphonedb.org/
Bio-Rad CFX Maestro 1.1 V4.1.2435.1219	Bio-Rad	https://www.bio-rad.com/en-us/category/qpcr-analysis-software?ID=42a6560b-3ad7-43e9-bb8d-6027371de67a
Other		
Bullet Blender 24	Next Advance	https://www.nextadvance.com/bullet-blender-homogenizer/

(Continued on next page)

Continued

REAGENT or RESOURCE	SOURCE	IDENTIFIER
KingFisher Flex 96 System	ThermoFisher Scientific	https://www.thermofisher.com/us/en/home/life-science/dna-rna-purification-analysis/automated-purification-extraction/kingfisher-flex.html
CFX96 Touch Real-Time PCR Detection System	Bio-Rad	https://www.bio-rad.com/en-us/product/cfx96-touch-deep-well-real-time-pcr-detection-system?ID=LZJTUJ15

RESOURCE AVAILABILITY

Lead contact
Further information and requests for resources and reagents should be directed to and will be fulfilled by the lead contact, Shelli Farhadian (shelli.farhadian@yale.edu).

Materials availability
This study did not generate new unique reagents.

Data and code availability
Datasets for bulk (GSE171995) and single cell (GSE171381) RNA sequencing in the paper are available at GEO.

The code generated during this study are available at:

https://github.com/archavan/covid-placenta

Additional Supplemental Items are available from Mendeley Data at:

https://data.mendeley.com/datasets/v6bgbwf3td/1

EXPERIMENTAL MODEL AND SUBJECT DETAILS

Human subjects
All women who presented to Yale New Haven hospital for delivery underwent routine clinical testing for SARS-CoV-2 during the study period (March 27, 2020 to June 1, 2020). Women who were admitted to Yale New Haven Hospital Labor and Birth during the study period and who were positive for SARS-CoV-2 by nasopharyngeal swab RT-qPCR at the time of or in the one month prior to delivery hospitalization were approached for consent to donate additional tissue for research studies through the Yale IMPACT study (Implementing Medical and Public Health Action Against Coronavirus in CT). These participants provided informed consent for research studies of donated placental and blood tissue. They provided additional clinical information and were included in RNA sequencing and PCR analyses of placenta. In addition, for the histological analyses, we performed chart review to retrospectively identify all women who were diagnosed with SARS-CoV-2 infection by NP swab RT-qPCR at the time of or in the one month prior to delivery during the study period, and who had placental sections available for histological review. Pre-pandemic (before 2019) histological controls were selected from pathology files at Yale New Haven Hospital and matched to the COVID-19 placental cases by maternal age, gestational age, and maternal co-morbidities. Additional SARS-CoV-2 uninfected women (as determined by negative RT-qPCR testing of nasopharyngeal swab) were recruited during the study period and provided informed consent to donate placenta tissue to serve as uninfected controls for transcriptomic studies. Placentas from uninfected controls were confirmed negative by RT-qPCR.

The study was approved by the Yale Institutional Review Board (protocol #2000027690 and 2000028550).

Pathology files at Yale New Haven Hospital were searched for placentas corresponding to cases of maternal COVID-19 during the study period. All available placental cases were included in the histological study. Additionally, pathology files were searched for placentas from mothers without SARS-CoV-2 infection (pre-June 2019) to serve as historical controls. These controls were matched to study cases for maternal age, gestational age and maternal comorbidities. A total of 27 cases and 10 matched controls were assessed histologically. Of those, one case was of a dichorionic diamniotic twin pregnancy. The placentas of this twin pregnancy demonstrated extremely similar microscopic features and identical pathologic scores; thus, they were together considered as a single case in the statistical analysis.

Further information related to the subjects can be found in Table 1.

For healthy control tissues and placental cell isolation, samples from normal term placentas were collected anonymously from healthy patients undergoing elective repeat Cesarean sections. All women who provided term placental samples signed an informed consent (Yale IRB protocol 1208010742).

First and second trimester specimens from the elective termination of pregnancy, ranging from 7 to 15 weeks of gestation (based on last menstrual period), were collected from otherwise healthy women with no known genetic or other abnormalities, as previously described.[93] All women who provided first and second trimester placentas signed an informed consent (protocol #021-06-972) approved by the ethical committee of the Bnai Zion Medical Center, Haifa, Israel under Helsinki convention guidelines. Placentas of gestational age 18 to 23 weeks were obtained from non-genetic healthy terminations through the University of Pittsburgh Biospecimen Core (IRB#: PRO18010491).

Primary cell cultures
Isolation of Hofbauer cells and cytotrophoblasts from healthy term placentas was performed as previously described.[94] Placentas from uncomplicated term pregnancies were brought to the laboratory within 30 minutes following elective cesarean section without labor at Yale-New Haven Hospital and processed immediately. Inclusion criteria included maternal BMI < 40, singleton pregnancy, neonatal birth weight > 2500 g, and > 10th percentile for neonatal weight. Exclusion criteria included multiple gestations, evidence of infection, any significant comorbidities (i.e., chronic hypertension, diabetes mellitus, autoimmune disease, congenital heart disease, chronic severe asthma, thrombophilia), placental abruption or vaginal bleeding during pregnancy, psychiatric conditions, use of medications associated with preterm delivery, and substance use during delivery. Primary placental cells were maintained in F12:DMEM with 10% FBS supplemented with antibiotic/antimycotic.

Cell lines
BeWo cells were maintained in F12K Kaighn's modified media, HTR-8/SVneo cells in RPMI media, and Vero E6 cells in F12:DMEM media, all with 10% FBS and antibiotic/antimycotic.

METHOD DETAILS
SARS-CoV-2 detection in placenta by RT-qPCR
Placenta samples were homogenized and centrifuged before nucleic acid was extracted using the MagMax Viral/Pathogen Nucleic Acid Isolation Kit. RNA was

isolated from cells infected with SARS-CoV-2 *in vitro* using the QIAGEN RNeasy Mini Kit.

SARS-CoV-2 was detected using a modified RT-qPCR assay with the N1, N2, and human RNase P (RP) primer-probe sets developed by the CDC and the NEB Luna Universal Probe One-Step RT-qPCR kit on the Bio-Rad CFX96 Touch Real-Time PCR Detection System.[95] Each sample was extracted and tested in duplicate to confirm results. Placenta samples were considered positive by RT-qPCR if cycle threshold (CT) values for N1 and N2 were both < 38, and with any value of RP. Samples were considered negative if N1 and N2 > 38, and RP < 38. Samples were considered invalid if N1 and N2 > 38 and RP > 38.

SARS-CoV-2 S1 spike protein IgM and IgG serology testing

ELISA assays for IgG and IgM antibodies toward SARS-CoV-2 were performed on plasma as described by Amanat et al.[96] Screening was conducted on a total of 367 plasma samples from all SARS-CoV-2-positive patients enrolled.

In short, Triton X-100 and RNase A were added to serum samples at final concentrations of 0.5% and 0.5 mg/ ml respectively and incubated at room temperature for 30 min before use to reduce risk from any potential virus in serum. Then, 96-well MaxiSorp plates (Thermo Scientific 442404) were coated with 50 μL per well of recombinant SARS-CoV-2 S1 protein (ACROBiosystems S1N-C52H3-100 μg) at a concentration of 2 μg/ml in PBS and were incubated overnight at 4°C. The coating buffer was removed, and plates were incubated for one hour at room temperature with 200 μL of blocking solution (PBS with 0.1% Tween-20, 3% milk powder). Serum was diluted 1:50 in dilution solution (PBS with 0.1% Tween-20, 1% milk powder) and 100 μL of diluted serum was added for two hours at room temperature. Plates were washed three times with PBS-T (PBS with 0.1% Tween-20) and 50 μL of HRP anti-Human IgG Antibody (GenScript A00166, 1:5000) or anti-Human IgM-Peroxidase Antibody (Sigma-Aldrich A6907, 1:5000) prepared in dilution solution were added to each well. After one hour of incubation at room temperature, plates were washed six times with PBS-T. Plates were developed with 100 μL of TMB Substrate Reagent Set (BD Biosciences 555214) and the reaction was stopped after 12 minutes by the addition of 100ul of 2 N sulfuric acid. Plates were then read at a wavelength of 450 nm and 570 nm.

The cut-off values for sero-positivity were determined as 0.392 and 0.436 for anti-S1-IgG and anti-S1-IgM, respectively. Eighty pre-pandemic plasma samples were assayed to establish the negative baselines, and these values were statistically determined with confidence level of 99%.

Histopathological analysis of placenta

Freshly collected specimens were fixed in 10% neutral buffered formalin (NBF) for at least 24-48 hours and embedded in paraffin, after which 5 μm sections were placed on coated glass slides designed for H&E staining and immunohistochemistry (IHC) processing.

For historical specimens, pathology files at Yale New Haven Hospital were searched for placentas corresponding to cases of maternal COVID-19 during the study period. All available placental cases were included in the histological study. Additionally, pathology files were searched for placentas from mothers without SARS-CoV-2 infection (pre-June 2019) to serve as historical controls. These controls were matched to study cases for maternal age, gestational age and maternal

comorbidities. A total of 27 cases and 10 matched controls were assessed histologically. Of those, one case was of a dichorionic diamniotic twin pregnancy. The placentas of this twin pregnancy demonstrated extremely similar microscopic features and identical pathologic scores; thus, they were together considered as a single case in the statistical analysis. All placentas received with a requisition form for pathologic evaluation were immediately fixed in 10% neutral buffered formalin for three days. A total of six sections inclusive of at least two full thickness sections, peripheral membranes and umbilical cord were submitted for histologic examination.

Two pathologists (LI and RM) blinded to patient information and diagnostic report independently scored all H&E stained placental tissue for villitis (absent, low-grade or high-grade; if low-grade, focal or multifocal and if high-grade, patchy or diffuse), intervillositis (absent or present), increased intervillous fibrin (absent or present, defined as intervillous fibrin occupying > 10% of a full thickness section on 20x low-power magnification), chorioamnionitis (absent or present; if present, maternal and fetal inflammatory responses were staged and graded), fetal and/or maternal vascular malperfusion (absent or present; if present, a histologic description was recorded) and increased decidual lymphocytes (absent or present, defined as clusters of > 10 lymphocytes in > 3 foci in the placental disc and/or peripheral membranes). Diagnostic criteria for villitis, chorioamnionitis, fetal vascular malperfusion (FVM) and maternal vascular malperfusion (MVM) followed those reported in the Amsterdam placental workshop group consensus statement.[97] Cases with discrepant scoring results were reviewed and re-scored by both pathologists simultaneously. Results were correlated with maternal, fetal and placental COVID-19 status.

ACE2 immunohistochemistry

Following dissection, placental tissue was rinsed in PBS and fixed in 10% neutral buffered formalin for 48-72 hours. Tissues were paraffin-embedded and cut into 5 μm thickness sections by Yale Pathology Tissue Services. The following rabbit polyclonal antibodies were used: anti-ACE2 (Abcam, Cambridge, MA, ab108252, used at 1 μg IgG/ml); and, as a negative control, normal rabbit serum (Sigma-Aldrich, St. Louis, MO, R9133, used at 1 μg IgG/ml). Antibody concentrations were chosen to produce strong staining in the positive cellular structures without background staining.

Slides were immunohistochemically stained as previously described[98] using the MACH2 Rabbit HRP-Polymer system (Biocare Medical, RHRP520L, Pacheco, CA) to mark the sites of antibody binding with a brown deposit. All buffers contained Tween20 (Sigma-Aldrich, P1379) to facilitate uniform application of all reagents and 0.1% bovine serum albumin (Sigma-Aldrich, A9647) to block background staining. Paraffin sections were heated for 30 minutes at 60°C and treated with xylenes followed by rehydration in decreasing concentrations of ethanol (100%, 90%, 80%, 70%). After deparaffinization, antigen retrieval was performed by heating the slides in citrate buffer (pH 6.0) to [3] 95°C for 60 minutes using an Oster model 5712 food steamer. The citrate buffer was then allowed to cool to a temperature of 28°C before the slides were removed. Endogenous peroxidase activity was blocked by incubation in 0.03% hydrogen peroxide in ddH$_2$O for 30 minutes. The slides were drained and primary antibody was applied overnight at 4°C. After washing, the secondary polymer was applied according the Biocare MACH2 system instructions. The chromogen step utilized the Biocare Betazoid DAB Chromagen kit (BDB2004) for exactly 5 minutes at room temperature. Slides were counterstained with hematoxylin, decolorized with 4% acetic acid, and fixed with Li$_2$CO$_3$ for 40 s. The slides were then dehydrated in increasing concentrations of ethanol, cleared

with xylenes, and mounted with VectaMount permanent mounting medium (Vector Laboratories H-5000). To minimize run-to-run variability, replicate samples were stained simultaneously with one antibody. Positive control sections from a de-identified normal human kidney were analyzed concurrently with each batch of slides.

For quantification of immunoreactivity, slides were inspected microscopically using a raster pattern to ensure that the entire histologic section was examined. A modified histology score[99] was calculated by multiplying the percentage of trophoblasts that stained by the average staining intensity (ranging from 0-3), resulting in H-scores from 0 and 300.

Primary cell isolations from placentas

Isolation of Hofbauer cells and cytotrophoblasts from healthy term placentas was performed as previously described.[94] Placentas from uncomplicated term pregnancies were brought to the laboratory within 30 minutes following elective cesarean section without labor at Yale-New Haven Hospital and processed immediately. Inclusion criteria included maternal BMI < 40, singleton pregnancy, neonatal birth weight > 2500 g, and > 10th percentile for neonatal weight. Exclusion criteria included multiple gestations, evidence of infection, any significant comorbidities (i.e., chronic hypertension, diabetes mellitus, autoimmune disease, congenital heart disease, chronic severe asthma, thrombophilia), placental abruption or vaginal bleeding during pregnancy, psychiatric conditions, use of medications associated with preterm delivery, and substance use during delivery.

Villous tissue was dissected, minced, and rinsed with PBS. Minced tissue was subjected to sequential enzymatic digestions in a solution of 0.25% trypsin and 0.2% DNase I at 37°C. Undigested tissue was removed by passage through gauze and a 100-μm sieve. Cells were resuspended in DMEM:F12 media with 10% FBS and 1% antibiotic/antimycotic.

Cytotrophoblasts were separated on a discontinuous gradient of Percoll (50%/45%/35%/30%) by centrifugation at 1000 x g for 20 minutes at room temperature. Cells migrating to the 35%/45% Percoll interface were recovered by centrifugation at 300 x g for 10 minutes at room temperature and immunopurified by negative selection using mouse anti-human CD9 antibody and mouse anti-human CD45 antibody. Following incubation with goat anti-mouse IgG-conjugated Dynabeads, contaminating cells were removed by exposure to a magnet.

Hofbauer cells were isolated from further digestion of trypsin-treated tissue with collagenase A and DNase I. Cells were pelleted, resuspended in RPMI, and loaded onto a discontinuous Percoll gradient (40%/35%/30%/20%) and centrifuged for 30 minutes. Cells from the 20%/25% to 30%/35% interfaces were combined and immunopurified by negative selection using sequential treatment with anti-EGFR and anti-CD10 antibodies conjugated to magnetic beads. Cells from the supernatant were plated and after 1 hour of incubation, floating and weakly adherent cells were removed.

Fibroblasts were obtained from cells removed during negative immunoselection of cytotrophoblasts and Hofbauer cells. Bead-cell mixtures were washed and cultured in media until confluency was reached. Following trypsinization of first passage cells, magnetic beads with attached cells (~10% of population) were removed with a magnet. Passage 3 fibroblasts were used for experiments.

SARS-CoV-2 infections *in vitro*

Primary placental cells were with icSARS-CoV-2 mNG[20] infected at an MOI of 5 for one hour at 37°C. Following infection, cells were washed three times in PBS before adding fresh media. At the indicated time points, cells were washed three times in PBS and collected in Trizol (Invitrogen).

Immunofluorescence sample preparation and imaging

Placental cells on coverslips were fixed in fixed in 4% paraformaldehyde for 24 hours. Coverslips were blocked and permeabilized in 3% BSA (Sigma) and 0.1% Triton X-100 (American Bioanalytical). Each sample was incubated overnight with anti-SARS-CoV-2-NP rabbit polyclonal antibody (GeneTex # GTX135357) at a dilution of 1:200. After washing in PBS, coverslips were incubated for 1 hour in a 1:500 dilution of Alexa 594 anti rabbit secondary antibody (Jackson ImmunoResearch 711-585-152), washed again in PBS and treated with 1 µg/mL Hoechst 33342 for 10 min and washed a final time in PBS. Samples were then mounted in DABCO/glycerol mounting media (Sigma) and imaged on a Leica Sp8 Laser Scanning Confocal Microscope equipped with a 40x N.A. 1.3 HC PL APO CS2 objective. Images are displayed as maximum intensity projections of z stacks and a color bar is given in arbitrary digital units.

Preparation of decidua and placental villi for bulk and single-cell sequencing

Placentas were collected from Yale-New Haven Hospital and transferred to the laboratory for processing. Placental villi were isolated by sampling from midway between the chorionic and basal plates of the placenta. The decidua parietalis was isolated from the chorioamniotic membranes as previously described.[100] The chorioamniotic membranes were dissected, rinsed in PBS, and placed with the chorion facing upward. Blood clots were removed using fine-point forceps and membranes were rinsed in PBS. A disposable cell scraper was used to gently remove the decidual layer from the membrane.

Dissected tissues were rinsed thoroughly in PBS and minced with scissors in a tissue digestion buffer of Liberase TM (0.28 WU/ml) and DNase I (30 µg/ml) in HBSS with Ca^{2+} and Mg^{2+}. Finely minced tissue was enzymatically digested at 37°C for 1 hour with agitation, pipetting, and further mincing every 10 minutes until disaggregated. The suspension was passed through sterile gauze, centrifuged at 1000 x g for 5 minutes at 4°C to pellet cells, and washed with fresh digestion buffer. After centrifugation, the supernatant was aspirated and the cell pellet was resuspended in ACK lysing buffer for 5 minutes. Cells were centrifuged and resuspended in RPMI media before filtering through a 70-µm mesh cell strainer.

Bulk RNA sequencing

Total RNA was prepared from freshly isolated placental villi dissected from clinical specimens and rinsed three times in PBS. Homogenization and nucleic acid extraction was performed using the MagMax Viral/Pathogen Nucleic Acid Isolation Kit. RNA was isolated from cells infected with SARS-CoV-2 *in vitro* using the QIAGEN RNeasy Mini Kit. Depletion of rRNA, library preparation, and sequencing on the Illumina HiSeq 2500 platform were performed at the Yale Center for Genome Analysis (YCGA).

FASTQ files from HiSeq 2500 were analyzed using Kallisto v0.46.1[88] using the "-b 100 and -t 20" options to obtain transcript abundances in TPM and estimated counts. The kallisto index used during transcript quantification was built (31bp k-mer length) from the *Homo sapiens* transcriptome GRCh38 downloaded as a FASTA

file from Ensembl (https://uswest.ensembl.org/index.html). Transcripts were annotated using the Bioconductor package biomaRt v2.40.5[89] in R v3.6.2.

Read counts for individual transcripts were summarized for gene-level analysis using the Bioconductor package tximport v1.12.3 with default parameters.[90] Differential expression analysis was performed using DESeq2 v1.24.0 with default parameters,[91] comparing all 3rd trimester samples by maternal status.

Single-cell RNA sequencing

Library preparation. Single-cell suspensions were loaded onto the Chromium Controller (10x Genomics) for droplet formation. scRNA-seq libraries were prepared using the Chromium Single Cell 3¢ Reagent Kit (10x Genomics). Samples were sequenced using the Illumina NovaSeq platform.

Data preprocessing and clustering. Sequencing results were demultiplexed into FASTQ files using the Cell Ranger (10x Genomics; v3.0.2) mkfastq function. Samples were aligned to GRCh38 10x genome and the count matrix was generated using the count function with default settings. Low quality cells containing < 500 or > 6000 genes detected were removed, as well cells with > 20% of transcripts mapping to mitochondrial genes. Genes that were present in less than 3 cells were excluded from analysis. Gene expression values were then normalized, log-transformed, and scaled. Single cell transcriptomes from COVID-19 cases and healthy controls were pooled prior to unsupervised cluster analysis. Seurat version 3.1.5 with R version 3.4.2 was used for normalization, dimensionality reduction, clustering, and UMAP visualization, while Seurat version 3.2.2[92] with R version 4.0.2[101] was used for all downstream analyses.

Cluster annotation. Preliminary annotation of all clusters was performed by the similarity of their gene expression to annotated cell types in published single cell RNA-seq datasets of human maternal-fetal interface.[29–31] For each cluster, mean of SCTransform-normalized[102] gene expression across cells was calculated using Seurat function AverageExpression and used as the cluster's average gene expression. Spearman correlation coefficients between the cluster's average expression and averaged expression of annotated cell types from all three reference datasets were calculated using the R function cor, and top three cell types with highest correlation coefficient were assigned as preliminary annotations of the clusters (Figure S7). These annotations were further refined through manual examination of cluster marker genes (identified using Seurat function FindAllMarkers with options only.pos = TRUE and logfc.threshold = 0.25). During manual refinement of annotation, tissue origin of the cells was also taken into account, i.e., whether majority of cells in a cluster come from villi samples or decidua samples. Clusters that are highly similar to each other and have the same final cell type annotation, were then merged, resulting in the final set of 21 annotated clusters.

Differential gene expression. For each annotated cluster, differentially expressed genes between control and COVID-19 samples were identified using Wilcoxon rank-sum test as implemented in the Seurat function FindMarkers. Genes that meet the following criteria were considered differentially expressed: absolute log (natural) fold-change of 0.4 (corresponding to at least 50% change in expression) and Bonferroni-adjusted two-tailed *p-value* less than 0.05.

Functional enrichment analyses. Two types of functional gene set enrichment analyses were performed, Interferome[37] and Metascape.[32] For Interferome analysis,

lists of differentially expressed genes in each cluster were searched against Interferome (version 2.01) with the default parameters except that the search was limited to human genes. Enrichment score for each cluster was calculated as the ratio between the observed fraction of differentially expressed genes found in Interferome database and the expected fraction, where the expected fraction is the ratio of total number of genes in the Interferome database over the total number of genes used in differential expression analysis. Enrichment *p-value*s were calculated from the hypergeometric distribution using the R function phyper. Functional enrichment with Metascape was performed on lists of differentially expressed genes using the web application.

Ligand-receptor interactions. Ligand-receptor interactions were inferred using CellPhoneDB[33] separately for cells from control and COVID-19 samples. CellPhoneDB version 2.1.4 was used with Python version 3.6. For computational efficiency both control and COVID-19 data were subsampled to 5000 cells each. CellPhoneDB output was read into R for data visualization. CellPhoneDB output file count_network.txt was used for visualization of number of interactions between pairs of cell types in Figure 5E. For visualization of individual ligand pair interactions in Figure S6, we selected interactions that are present in COVID samples (adjusted p value < 0.01) but absent in control samples.

QUANTIFICATION AND STATISTICAL ANALYSIS

Statistical details can also be found in figures, figure legends, and main methods. One-way ANOVA was used to compare clinical and demographic features between the three groups presented in Table 2. Chi-square tests were used for statistical comparisons of histologic features of cases versus controls. Differences were designated statistically significant when the p value was less than 0.05.

In Figure 2, ACE2 H-score was compared between cases and controls using the Mann-Whitney test. The linear regression line for ACE2 H score versus gestational age was fit using Prism (v8.0.1), which was also used to calculate 95% confidence intervals. The equation for the best fit line is $y = -6.149x + 287.6$.

For bulk RNA sequencing analysis, differential expression analysis was performed using DESeq2 v1.24.0 with default parameters.

For single-cell RNA sequencing analysis of each annotated cluster, differentially expressed genes between control and COVID-19 samples were identified using Wilcoxon rank-sum test as implemented in the Seurat function FindMarkers. Genes that meet the following criteria were considered differentially expressed: absolute log (natural) fold-change of 0.4 (corresponding to at least 50% change in expression) and Bonferroni-adjusted two-tailed *p-value* less than 0.05.

For Interferome analysis, enrichment p values were calculated from the hypergeometric distribution using the R function phyper. For Metascape analysis, functional enrichment was performed using the Metascape web application.